2017

Utilization of Landsat Imagery to Assess the Impacts of Oil and Gas Extraction on the Tazovsky Peninsula, Siberia

Nicholas B. Kline
University of Montana

UTILIZATION OF LANDSAT IMAGERY TO ASSESS THE IMPACTS OF OIL AND GAS
EXTRACTION ON THE TAZOVSKY PENINSULA, SIBERIA

By

NICHOLAS BERNARD KLINE

B.A. Geography, California State University Fullerton, Fullerton, CA, 2015

Thesis

presented in partial fulfillment of the requirements
for the degree of

Masters of Science
in Geography, Cartography and GIS

The University of Montana
Missoula, MT

August, 2017

Approved by:

Scott Whittenburg, Dean of the Graduate School
Graduate School

Dr. Anna E. Klene, Chair
Department of Geography

Dr. David Shively
Department of Geography

Dr. Brady Allred
College of Forestry and Conservation

Dr. Samuel Cushman
Unites States Forest Service

Kline, Nicholas B. M.S., Summer 2017   Geography

Utilization of Landsat imagery to assess the impacts of oil and gas extraction on the Tazovsky Peninsula, Siberia

Chairperson: Dr. Anna E. Klene

Abstract

Climatic warming of the Arctic is leading to landscape change through cascading biophysical feedbacks; development, such as oil and gas exploration and extraction, can accelerate or worsen these impacts. Due to restricted access to oil and natural gas fields, *in situ* environmental impact studies are only allowed in some regions. Satellite imagery analysis provides a mean for assessing impacts in areas with limited access. The Yamburg oil and gas field in western Siberia serves as a case study to assess the effects of infrastructure on an Arctic landscape.

This project quantifies the land-cover disturbance that occurred during the development and expansion of the Yamburg field. Google's recently developed, cloud-based image processing platform, Google Earth Engine, was used in conjunction with traditional Geographic Information System (GIS) analysis to detect, map, and quantify the impacts of infrastructure on the Tazovsky Peninsula between 1983 and 2016, utilizing imagery from the Landsat 4, 5, and 8 satellites. Landscape fragmentation metrics, the Normalized Difference Vegetation Index (NDVI), and change analysis quantified the impacts of extraction infrastructure on the surrounding landscape. As distance from the infrastructure and time since field establishment increased, the associated impacts decreased.

Table of Contents

Table of Figures

Table of Tables

Introduction

Climatic warming of the Arctic is leading to increased warming and thawing of the

permafrost underlying the tundra and taiga (Arctic Council 2004). Permafrost (perennially

frozen ground) is ground which has been colder than 0°C for at least two years, though typically

much longer (Muller 1943). Permafrost acts as an aquaclude, preventing water infiltration, and

limiting biogeochemical cycling to largely above the permafrost table (French 2013). Thawing

permafrost begins a chain of hydrologic and biogeochemical feedbacks which are further

impacted by development, such as natural resource exploration and extraction. Gas and oil

extraction are one such resource-driven encroachment.

Oil, natural gas, and gas condensates are a major driver of the Russian economy (Finland

Chamber of Commerce 2016). The Yamburg gas condensate field is one of the most productive

in Russia (Gazprom Dobycha Yamburg 2016). Located in the Tazovsky Peninsula, the Yamburg

field sits on ice-rich permafrost (Yakushev et al. 2000). Without careful engineering, oil and gas

development on permafrost landscapes can have impacts such as impeded drainage and

thermokarst development, potentially resulting in damage to infrastructure (Nelson et al. 2001;

Mazhitova et al. 2004; Larsen et al. 2008; Raynolds et al. 2014; Shiklomanov et al. 2017).

Due to restricted access to oil and natural gas fields, which are considered national

strategic resources in some locations and are private corporate holding in others, *in situ* studies

assessing the environmental impacts of development are not permitted in some regions,

especially by foreign researchers. Remote sensing provides one means of performing studies in

these areas. This study will utilize Google Earth Engine[1], ArcGIS[2], TerrSet [3]software, and

Landsat imagery to detect, map, and quantify landscape changes in the Yamburg field.

In 2007, faculty member Anna Klene and graduate student Jesse Wallace were allowed

access to the Yamburg field as part of an international academic field course. Wallace used this

as the field work for his thesis (2012) using satellite imagery to quantify Yamburg's impact on

the landscape between 1987 and 2007. Wallace referenced field data and interpreted imagery to

digitize the extent of infrastructure, and analyzed change within buffers at set intervals. As the

infrastructure expanded, the landscape became more fragmented, and differences in disturbance

and recovery could be seen between buffers. This study updates Wallace's original work by

extending the period of analysis to 2016, analyzing a larger study area, and using Google's

recently released raster-processing platform, Google Earth Engine, to incorporate additional

satellite imagery. Google Earth Engine allows for stacks of imagery to be easily analyzed

instead of the single scenes which had traditionally been used. The use of imagery stacks can

"allow long-term changes to be detected with greater sensitivity and reliability by comparison to

conventional two-date change detection" (Fraser et al. 2011) in both land-cover and vegetation

(Röder et al. 2008; Huang et al. 2009; Broich et al. 2011; Stueve et al. 2011; Kontgis et al. 2015).

---

[1] Google Earth Engine Team, 2015. Google Earth Engine: A planetary-scale geospatial analysis platform.
https://earthengine.google.com
[2] Environmental Systems Research Institute (ESRI) "ArcGIS Release 10.4." *Redlands, CA* (2017).
[3] Eastman, J. R. "TerrSet: Geospatial Monitoring and Modeling Software." *Clark Labs, Clark University* (2015).

Research Questions

These questions follow those of Wallace's (2012) in terms of assessing landscape fragmentation, quantifying change in vegetation greenness, and comparing these values over time to identify periods of disturbance and recovery.

1. To what extent has the landscape been fragmented by the development and expansion of the Yamburg oil and gas condensate field?

2. Can the maximum seasonal Normalized Difference Vegetation Index (NDVI) detect any changes in greenness of tundra vegetation adjacent to infrastructure development on the Tazovsky peninsula?

3. Can comparison of the changes in maximum seasonal NDVI values over time identify both the initial disturbance and recovery of vegetation following infrastructure development?

Study Area

The Yamburg oil and gas condensate field is located within the Yamalo-Nenets Autonomous District (YAO) in west Siberia (Figure 1). Spanning 750,300 km², the YAO has a population of 534,100; 446,900 live in urban centers and 87,200 in rural areas (Yamalstat.ru 2016). The urban centers originated primarily to serve the resource extraction industry. Natural gas extraction is the primary economic driver in the region, which produces 34% of Russia's total gas production (Gazprom Dobycha Yamburg 2016).

The study area was constrained to a box surrounding the extent of the roads and pads associated with infrastructure of the Yamburg field (Figure 1). The Tazovsky Peninsula is 18,723 km² with the study area occupying 9,164 km² or 49% of the entire peninsula. The region is underlain by permafrost, with vegetation a mix of moss, lichen, sedges, and dwarf shrubs (Forbes 1997). The mean monthly temperatures within this region ranges from -24°C in January to +14°C in July, with mean precipitation of 209 mm/yr (Russian Climate Server, 2016).

Anthropogenic impacts in the region have been of interest since the establishment of natural resource extraction infrastructure. Pollution, mining waste, oil spills, and loss of habitats are among the main impacts caused by extraction industries (Rees and Williams 1997).   A series of studies have been performed to assess impact of pollution on vegetation in the region, primarily on the neighboring Yamal Peninsula (Rees and Kapitsa 1994; Rees and Williams 1997; Saich et al. 2001; Toutoubalina and Rees 2010; Bashkin et al. 2017). Though there are not studies within the Tazovsky Peninsula, it can be assumed that similar pollution is occurring within the Yamburg field and impacting land cover as in other parts of Siberia with similar development (Vilchek, 2000).

Development of the Yamburg oil and gas field began in the early 1980s. Local sand and soil from the Yamburg area was used for much of the construction and maintenance material. Thus the spectral signature of roads, construction pads, bare soil, and sand bars will be essentially identical, making differentiating roads and pads from the natural surrounding landscape difficult based upon spectral information alone.

Methods

The following sections outline the methods used in this research. Background information for each research question is given at the beginning of its section. The techniques used to gather, create, and analyze the vector data, and the fragmentation metrics and analysis are discussed first. Then the gathering, processing, and analysis of the raster NDVI datasets follows.
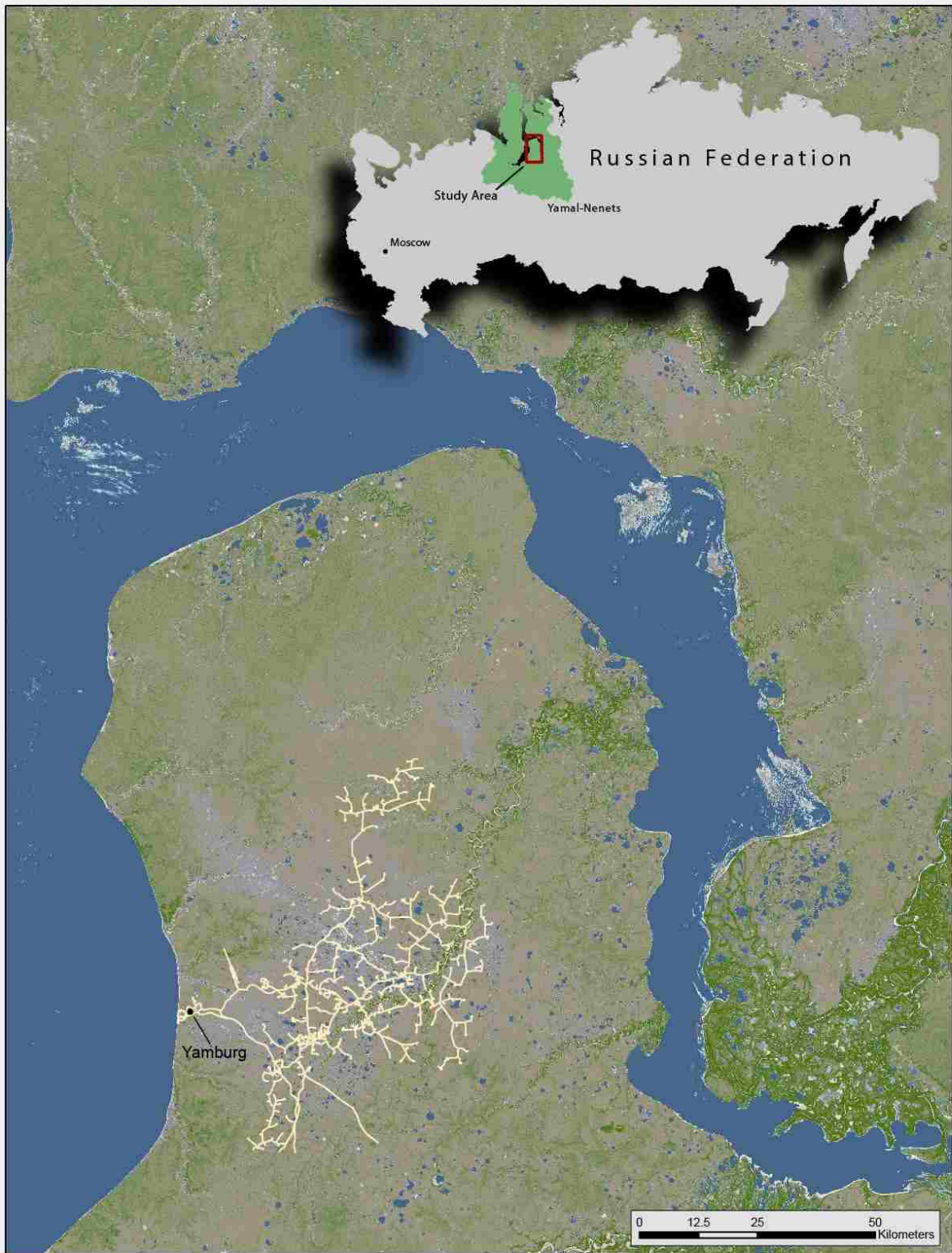
Figure 1. The study area on the Tazovsky Peninsula, Siberia. Infrastructure in 2016 is shown in yellow on top of the 10 July 2016 Landsat 8 true-color image (bands 2, 3, and 4).

Vector Infrastructure Data

Since this study is an extension of earlier research by Wallace (2012), his initial vector data were available for comparison and updated using the following protocol for each year. Based on visual interpretation of the Landsat imagery, roads, drilling pads, and refining facilities were hand digitized in ESRI's ArcMap. The Yamburg field has over 1000 km of feeder pipelines about 0.5 m in diameter, and almost 500 km gathering pipelines ~1.0-1.4 m in diameter, which may be elevated on pilings, laid on the ground and covered with soil, or buried up to 2 m deep (Seligman, 2000). However, due to the 30 m resolution of the imagery, pipelines were not included since they could not be seen clearly enough to map and might or might not change the land-cover due to their installation. Visible pads for drilling, buildings, and similar infrastructure were digitized as polygons. Roads were digitized as lines along the center, then buffered by 15 m to a width to 30 m, and then merged with the pads and refining facilities. Repeated for each year of study, the resulting vector data comprised the infrastructure "footprint".

A series of seven, ringed buffers were created around each years' infrastructure footprint at 30 m intervals (30, 60, 90, 120, 150 m), with coarser buffers at 300 and 600 m intervals (Wallace, 2012). This followed Walker and Everett. (1987) and Myers et al. (2006) who examined the impact of road dust on the physio-chemical characteristics of the soil and vegetation community composition on Alaskan tundra, finding impacts on vegetation composition and soil pH extending 300 m from roads.

Four, 100 km² control areas were placed around the furthest extent of the infrastructure footprint in 2016 in areas believed to be undisturbed. The control areas were placed based upon visual interpretation in areas across a gradient ranging from dry to wet (Figure 2).
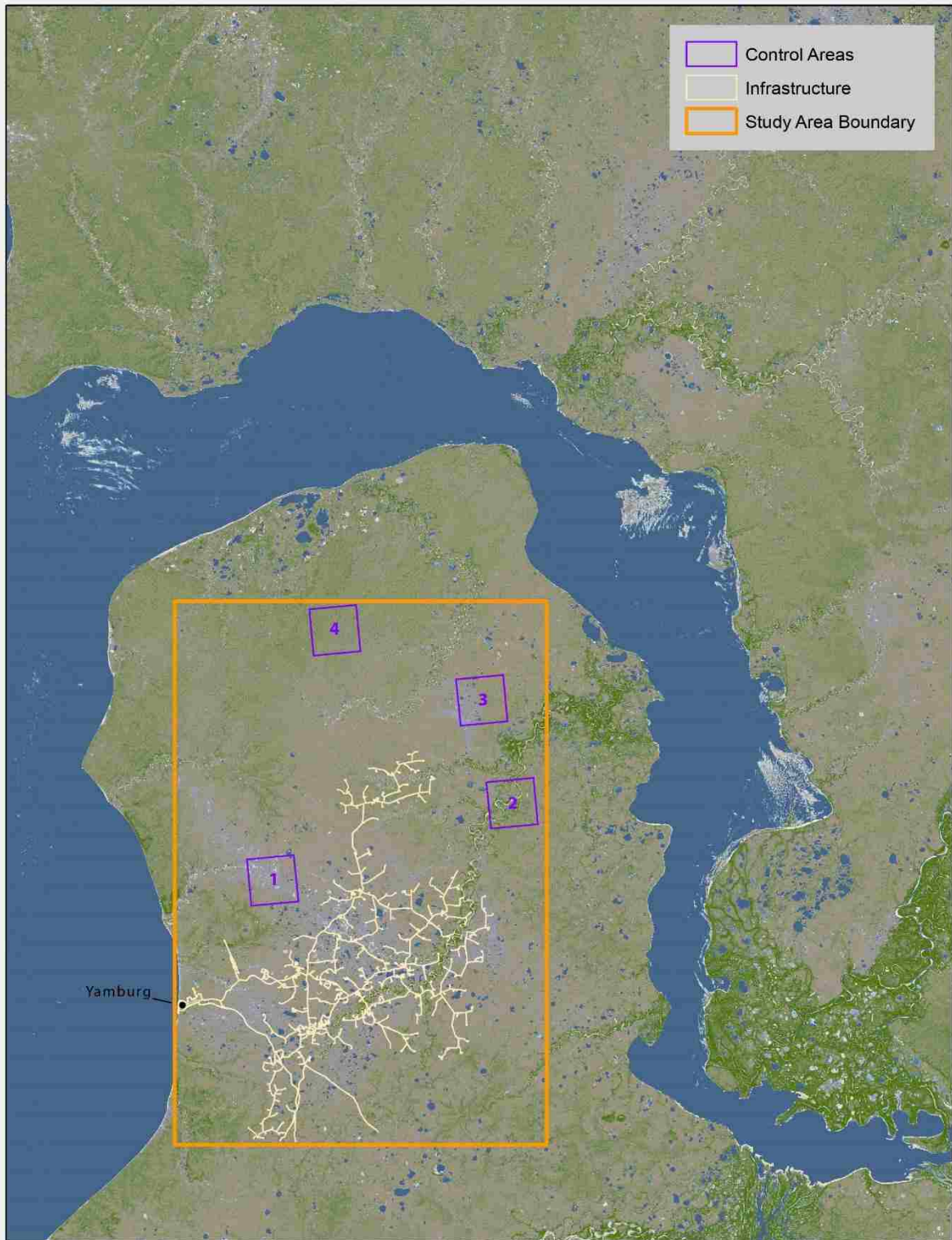
Figure 2. Map of study area boundary (orange outline) and control sites (purple outline). The infrastructure footprint as of 10 July 2016 is shown in yellow on top of the 2016 Landsat 8 true color (bands 2, 3, and 4) image.

Fragmentation Analysis

Landscape ecology studies the interaction between environmental patterns and ecological processes (Turner 1989). These spatially distributed patterns connect an organism's actions to its surrounding habitat. Anthropogenic development can "disrupt the structural integrity of landscapes and is expected to impede ecological flows" (McGarigal 2015). FRAGSTATS, a spatial pattern analysis program, can be used to calculate metrics which quantify the structure and spatial heterogeneity of the landscape (McGarigal 2015). This research attempts to quantify the extent and magnitude of change over time on the entire Tazovsky Peninsula using a binary categorization of undeveloped land and infrastructure.

Fragmentation studies primarily address the influence of anthropogenic activities on habitats (Andren 1994; Fahrig 1997; Harrison et al. 1999; Schneider 2001). Weller et al. (2002) used fragmentation analysis to quantify the impact of oil and gas extraction infrastructure within the Upper Green River Basin of Wyoming. By combining available reference data and hand digitization, an infrastructure footprint (pipelines, roads, drilling pads, etc.) was created. The results of the analysis quantified the impacts of infrastructure with a total habitat loss of four percent in the basin, covering 18 km² (7 mi^2) of the 430 km² (166 mi^2) study area.

Southworth et al. (2004) compared using land-use classification techniques and vegetation indices for mapping land cover and land fragmentation in western Honduras. A series of four Landsat 5 images were used. NDVI of each image was analyzed for threshold values which distinguished between forested and non-forested areas. The study concluded that patch size, clustering, and characteristics reflected the increase or decrease of economic activity in the region.

Cushman and Wallin (2000) examined the rate and amount of landscape change between 1972 and 1992 using Landsat imagery in the Sikhote-alin Mountains, Russia. Single images from 1972 and 1992 were classified for dominant land-cover. Eleven metrics were used to quantify change between the two years, resulting in an average of 0.66% of the landscape disturbed each year between 1972 and 1992.

This study will utilize a combination of methods and metrics (Table 1) from Cushman and Wallin (2000), Southworth et al. (2003), and Weller et al. (2002) to examine fragmentation. These metrics were selected because of their ability quantify and describe the fragmentation due to infrastructure growth. *Class Area, Landscape Percentage, Patch Count, Edge Density, Largest Patch,* and *Correlation Length* (radius of gyration in FRAGSTATS) are area metrics which deal with the number and size of the patches. *Core Area* quantifies the area within the patches, but because of the binary categorization used here, this will be the same as Class Area. Edge Density is the total length of all the patches, and due to the binary categorization used will have the same length for both categories as the only boundary is between them.

Metric	Description
Class Area (CA)	Total area occupied by each class
Core Area*	Total area within each patch
Landscape Percentage (PLAND)	Percentage of analysis area occupied by given patch type
Patch Count (NP)	Total number of individual patches by class
Largest Patch Index (LPI)	Area of the largest patch in the analysis area
Edge Density	Edge length of a given patch
Correlation Length	Physical connectedness of the landscape

* Because only 2 categories were used Class Area and Core Area are the same.

Table 1. Fragmentation metrics calculated in this study using Fragstats (2012).

Raster Data Preparation

<u>Google Earth Engine</u>

Google Earth Engine (GEE) is a powerful cloud-based raster analysis platform coupled to a growing archive of imagery gathered from NASA's Earth Observing Satellites (Landsat, MODIS, etc.) and ESA's Sentinel satellites, among other sources. This free, highly accessible system provides a user-friendly interface to "enable petabyte-scale, scientific analysis and visualization of geospatial datasets" (Gorelick 2013). Though it is mainly being used to perform time-series analysis, the computational power of Google's cloud network can calculate complex algorithms in minutes. The system enables researchers to allocate more time to analysis rather than gathering and preparing data. Because of its recent and on-going development, published GEE-based research is scarce. As of May 2016, there was a large library of standard processing and analysis tools built into the platform. Once coded, additional processing and analysis tools will be implemented, increasing the overall functionality of GEE.

Initial GEE-based studies generally produce comparable results to traditional methods, but allowing for larger datasets to be included in analyses. Dong (2016) examined shifts in rice phenology to map and inventory paddies in northeast Asia with similar accuracies compared to traditional methods. In Australia, Johansen (2015) found that GEE was comparable to traditional methods for mapping land-cover categories. Several studies have found that GEE was an effective method for mapping human movements and settlement development (Patel 2014; Trianni 2014).

For this research, Google Earth Engine served as the main data repository and image stack manipulation software, allowing for the query, processing, and download of required imagery. Imagery spans 28 years in roughly 10 year intervals from 1988 to 2016. Each interval,

or time slice, used one composite image representing maximum seasonal greenness for that slice.

Vegetation

Phenology is the study of the seasonal life stages of plants and animals (Morren 1843). In arctic tundra environments, vegetation is dominated primarily by low-growing shrubs, mosses, and lichen (Walker et al. 2002). Due to specific arctic plant adaptations, snow cover and temperature are integral to phenological cycles (Chapin et al. 1983; Billings 1987). For many Arctic plants, photosynthesis begins as low as 0°C and reaches optimum productivity at 15°C (Billings 1987). During the transition into spring, an onset of photosynthesis called the "green wave" begins. By end of summer, the wave peaks and begins to decline as the growing season comes to a close and plants undergo senescence. This rise and fall of greenness can be detected by satellite sensors (Schwartz 1998; Reed et al. 2009).

The Moderate Resolution Imaging Spectroradiometer (MODIS) sensor captures daily images of the Earth at a pixel resolution of 250 to 1000 m over a range of wavelengths useful for detection of regional phenological shifts, such as the green wave (Cihlar et al. 2001; Kawamura et al. 2005; Brown et al. 2006). Previous studies utilized the MODIS 16-day NDVI product (Karlsen et al. 2007; Robin et al. 2008; Narasimhan et al. 2010; Zeng et al. 2011) and MODIS Daily Snow Cover Product (Narasimhan et al. 2010) to determine growing seasons in high latitudes. For the Yamburg study area, these two MODIS products, as well as the MODIS Land Surface Temperature product, were analyzed within GEE. The 15-year (2001–2016) record of each of these was examined and the mean for the respective daily or 16-day period over that time was calculated for the rectangular study area (Figure 2), graphed within GEE, and visually examined (Figure 3) to identify dates of the growing season. Julian dates 153 to 265 (June 2 to

September 22 most years) included the full growing season and were used as the beginning and end dates of potential Landsat imagery to be analyzed within GEE.
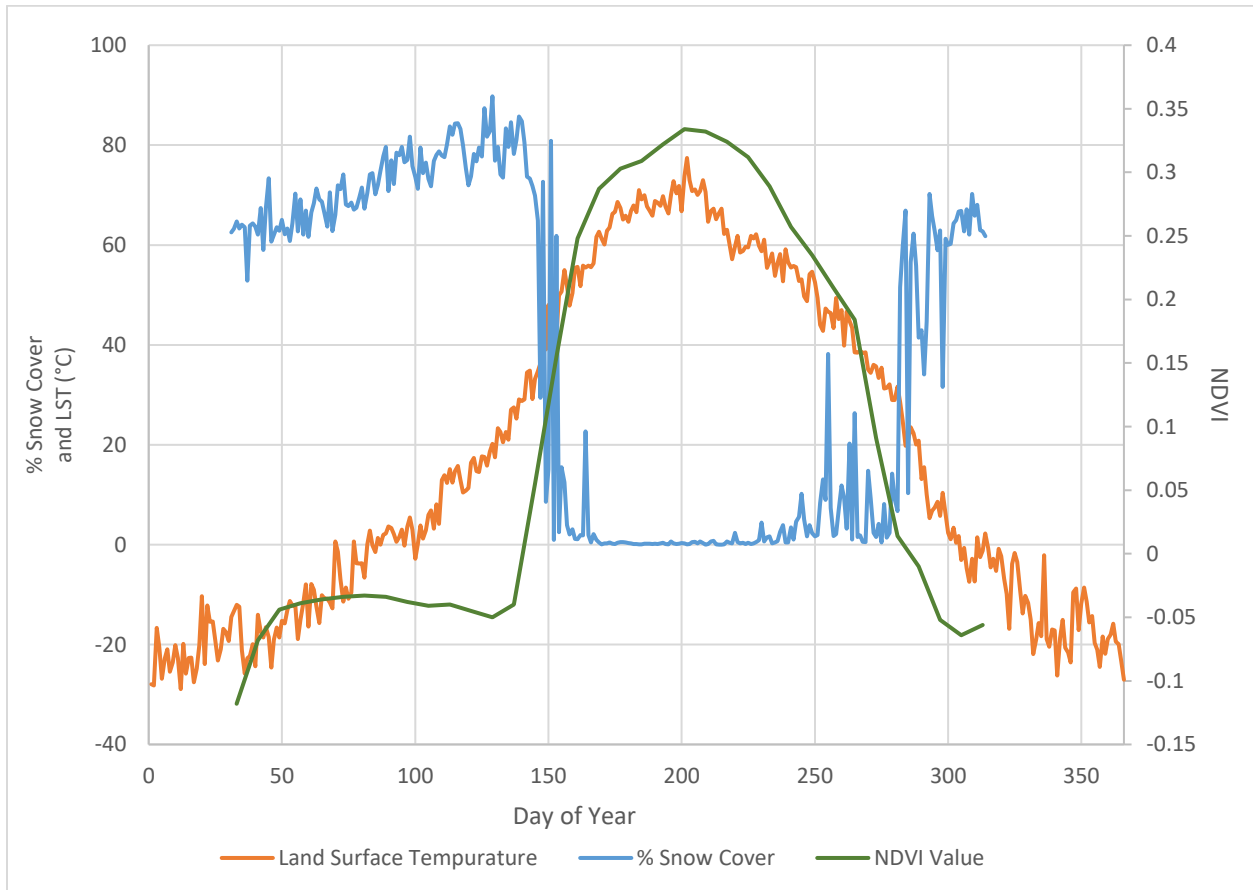
Figure 3. Graph of 2002 to 2016 MODIS land surface temperature (LST), MODIS snow cover, and MODIS NDVI values used to estimate growing season onset and cessation.

Landsat Imagery

To assess vegetation change surrounding the hydrocarbon extraction infrastructure, imagery from the Landsat program provided the longest archive, spanning from 1972 (Landsat 1) to present (Landsat 8). Due to Landsat's consistent spatial resolution of 30 m (from 1982 to present), similar spectral resolution between satellite versions, and wide use for mapping arctic

land cover (Walker et al. 1987; Fuller et al. 1994; Rees et al. 2003; Gong et al. 2012), robust comparisons through time can be made. Wallace's 2012 project included four time slices. This project added another, for a total of five slices: 1983, 1988, 1998, 2007, and 2016, spanning initial field development through current production (Table 1). These years were selected due to mid-season images being available at approximately 10-yr intervals. Imagery was queried and filtered to the growing season defined above. Landsat 7 imagery was not utilized because of the Scan-line Corrector (SLC) error on the sensor which resulted in missing data on every scene after May of 2003.

Satellite	Sensor	Year	Number of scenes
Landsat 4	MSS	1983	1
Landsat 4	TM	1988	24
Landsat 5	TM	1998	29
Landsat 5	TM	2007	29
Landsat 8	OLI	2016	48

Table 2. Satellite, sensor, year, and number of total scenes used of imagery used for analysis. The 1983 MSS image serves as a base year with only initial staging of equipment and material at a site on the west coast as development was beginning.

Normalized Difference Vegetation Index

One of the earliest and the most widely used ways of quantifying vegetation greenness is the Normalized Difference Vegetation Index (NDVI; Rouse et al. 1974). NDVI is the ratio of the difference between red and near-infrared (NIR) wavelengths,

$$NDVI = \frac{(NIR - RED)}{(NIR + RED)}$$

such that pixels with less green vegetation have values closer to 0 and more green vegetation are closer to +1. Values close to or just below 0 are typically water, and synthetic surfaces are between 0 and -1 (Rouse et al. 1974; Weier et al. 2000).

NDVI has been used to monitor disturbance and recovery in a variety of land-cover types (Viedma et al. 1997; Goetz et al. 2006; Masek et al. 2008; Beck et al. 2011; Schroeder et al. 2011; Lanorte et al. 2014). It was selected for this analysis due to its widespread, reliable application and known performance in the high latitudes. Goetz et al. (2005), Raynolds et al. (2008), and Zhou et al. (2003), among others, utilized NDVI in their studies looking at the impacts of regional warming trends on vegetation.

Image Analysis

The NDVI scenes within the growing season for each year were processed to select the maximum NDVI value, $NDVI_{max}$, for each pixel from the Landsat images available (Figure 4) within GEE. Maximum NDVI was selected for analysis because of its ability to "capture the dynamics of green vegetation and minimize problems with single-date data" (Agriculture and Agri-Food Canada) including clouds, haze, and scattering (Holben 1986; Mynenl et al. 1997; Zhou et al. 2001; Martinez and Gilabert 2009). Figure 5 shows the workflow used in GEE to select the highest NDVI value from each stack of imagery. The furthest edges of the control sites and the infrastructure layer were used to generate an area extent which eliminated the large stretches of undisturbed land north of the Yamburg field. This extent was exported and downloaded from GEE, generating the bounds of the study area (Figure 2).

In ArcMap, the vector data, including the infrastructure layer, buffers, and control sites were overlaid on the study area's $NDVI_{max}$ image (Figure 6). To address potential variability of NDVI values (Zhou et al. 2001), the mean of the $NDVI_{max}$ values, $\overline{NDVI_{max}}$ was calculated for each buffer and control site. These buffer values were graphed for comparison within each time slice.
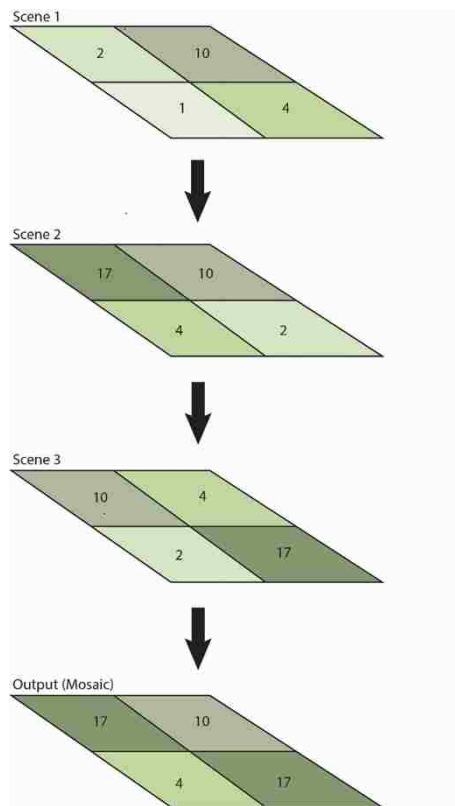
Figure 4. Illustration of selecting the maximum NDVI value per pixel from 3 scenes.

Figure 5. Illustration of mosaicking the imagery together based upon the maximum seasonal NDVI value. First all imagery within the growing season are selected. Clouds and water pixels are then masked out (second tile). NDVI was then computed for all images (third tile). Finally, a mosaic is created by selecting the maximum NDVI value per pixel from the stack of images.
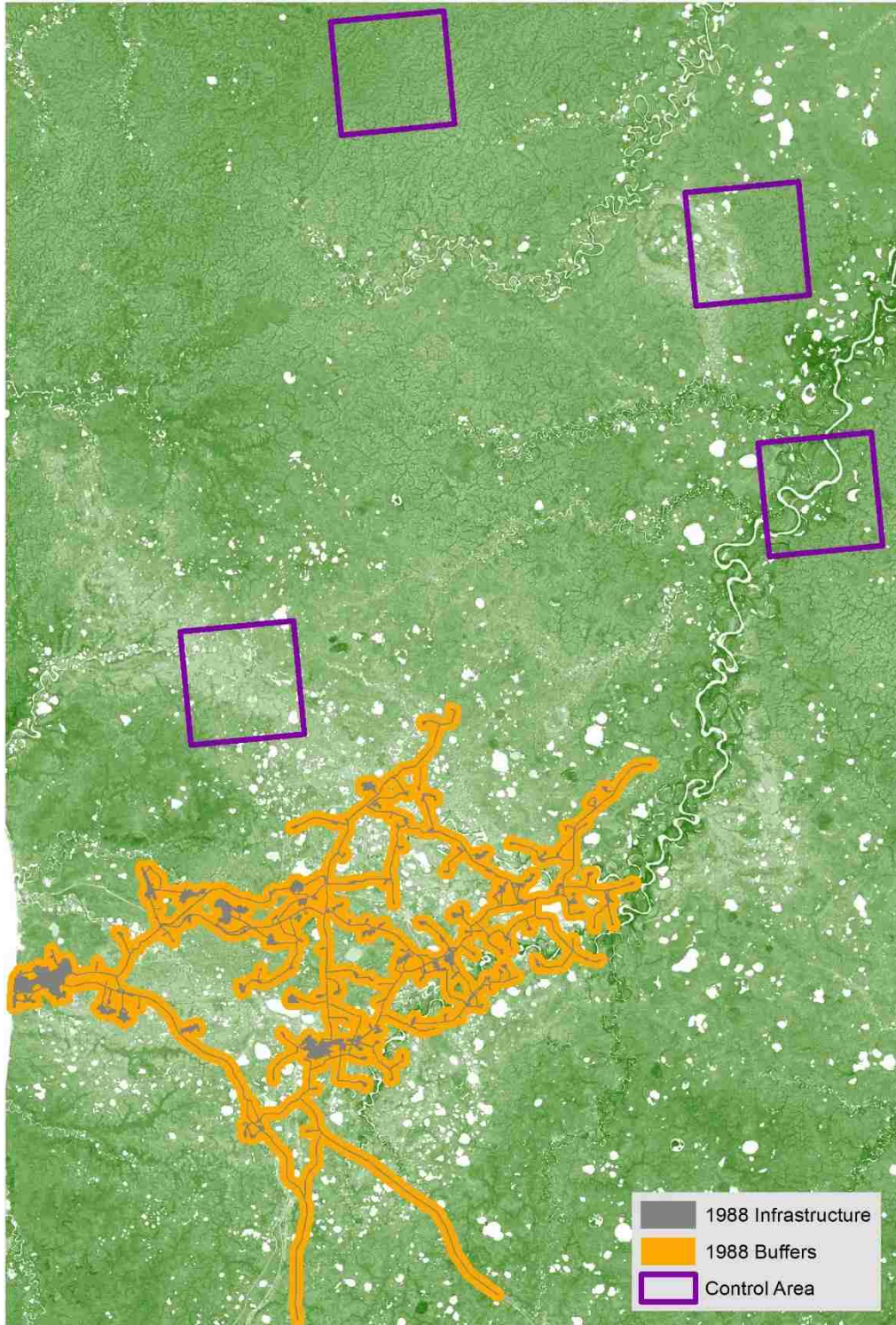
Figure 6. Image of maximum NDVI for 1988 showing infrastructure, buffers (to 600 m), and control areas.

Change Analysis

No attempt to do a traditional land-cover classification was performed because of restricted access to the site to gather ground-truth data, known confusion between the spectral signature of infrastructure and undisturbed bare ground, changes in lake color observed previously (Wallace, 2012), lack of a 30×30 m or finer land-cover map for the region, and Landsat's established diminishing land-cover classification accuracy finer than Anderson Level 1 categorization (tundra, desert, forest, etc.) in arctic regions (Anderson 1972; Nelson et al. 1984; Moore and Bauer 1990; Johnston and Barson 1993; Klemas 2001; Reese et al. 2002).

Instead, TerrSet's cross tabulation module was used to compare change in the normalized NDVI pixel values through time. To account for seasonal differences between years, the mean value of all the $NDVI_{max}$ pixels within the rectangular study area (0.43825, 0.46977, 0.45820, and 0.53420, for 1988, 1998, 2007, and 2016, respectively) was subtracted from each individual $NDVI_{max}$ pixel for that year. This normalized the data such that a wet year should not overwhelm the differences in greenness compared to a subsequent dry year. For this study, Terrset software was used to cross tabulate the change in normalized $NDVI_{max}$ pixel values between one time slice and the next. These were also aggregated within each buffer.

To aid analysis and see if changes in the extent of water were causing substantial changes in NDVI values through time, each normalized image was sliced by user-defined pixel values (based on manually sampling the imagery) into several land-cover categories broader than an Anderson Level 1 (Table 3). The resulting images were compared by cross-tabulation to the corresponding one for the next time slice. These classified change images were brought back into ArcMap and recategorized into positive (more greenness), negative (less greenness), or no change (Table 4) between years. This allowed visualization of change between time slices

(Figure 7; all change maps are shown in Appendix B). However, because of the known issues

mentioned above, analysis and interpretation was limited to the areas within the buffers around

infrastructure and the control areas.

Class	Description	Normalized NDVI$_{max}$ Values			
		1988	1998	2007	2016
1	Water	-0.84 to -0.45	-1.11 to -0.42	-0.92 to -0.43	-1.07 to -0.46
2	Sand/ Infrastructure	-0.45 to -0.20	-0.42 to -0.15	-0.43 to -0.13	-0.46 to -0.17
3	Sparse Vegetation	-0.20 to 0.00	-0.15 to 0.00	-0.13 to 0.00	-0.17 to 0.00
4	Light Green Vegetation	0.00 to 0.20	0.00 to 0.16	0.00 to 0.16	0.00 to 0.15
5	Dark Green Vegetation	0.20 to 0.45	0.16 to 0.38	0.16 to 0.44	0.15 to 0.33
0	Non-infrastructure	No Data	No Data	No Data	No Data

Table 3. Normalized NDVI$_{max}$ pixel values were reclassified into six land-cover classes by visual inspection of each time slice. Class 0 was when a pixel was not in a previous or subsequent buffer as the infrastructure was not yet or no longer present.

From Class	To Class	Change
1	3	Positive
1	4	Positive
1	5	Positive
2	3	Positive
2	4	Positive
2	5	Positive
0	2	Negative
3	2	Negative
4	2	Negative
5	2	Negative
2	1	Negative
3	1	Negative
4	1	Negative
5	1	Negative
0	1	No Change
0	3	No Change
0	4	No Change
0	5	No Change
1	0	No Change
3	0	No Change
4	0	No Change
5	0	No Change
4	5	No Change
5	4	No Change

Table 4. Reclassification of pixel change between land-cover classes. Categories of positive (more greenness), negative (less greenness), or no change were used for visualization of relative differences between years.
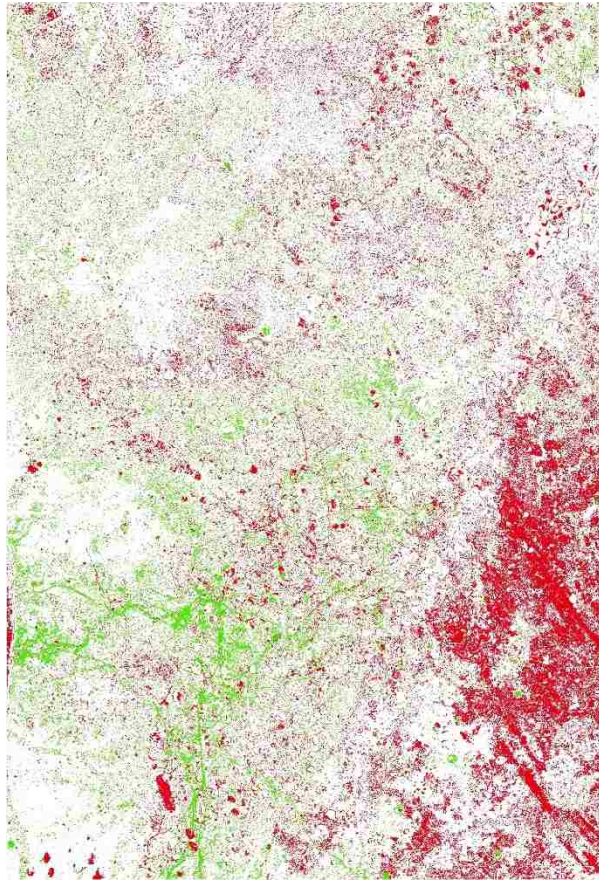
Figure 7. Example of a reclassified image of change between 1988 and 1998. Positive change (green) and negative change (red) based on categories in Table 7.

Results and Discussion

Fragmentation Results and Discussion

Landscape fragmentation analysis was performed on the full area of the Tavozsky Peninsula to gain insight on how infrastructure expansion impacted the landscape (Figure 8). Because of the lack of a suitable spatial resolution land-cover map, assessment of a land-cover-class fragmentation could not be performed beyond the binary categorization.

The fragmentation analysis (Table 5) showed that as the infrastructure spreads, the previously undeveloped landscape is increasingly patchy. In 1983 there was no visible development while resources for the establishment and expansion of the field were being stockpiled at the port in a "sub-surface tunnel which would be difficult to detect" (Wallace 2012) on Landsat imagery. After the initial field growth by 1988, the outward growth gradually slowed but continued, while infilling expanded, connecting the road and drilling pad network within the footprint (1998, 2007, and 2016). Some roads used during initial construction were abandoned and revegetated (Figures 7 and 9; Walker et al. 1987, Walker 1996, National Research Council 2003, Walker et al. 2014).

Class Area (CA) is the total area for each class (undeveloped and infrastructure). Between 1983 and 1988, the initial area of the field was 70.4 km² (Table 5 and Figure 8). By 1998, the area increased to 84.0 km², and the rate of expansion decreased such that in 2016 the area was 93.7 km². The *Landscape Percentage* (PLAND) metric reflects the gradual increasing trend of occupied area, from 0.38% of the entire peninsula in 1988 to 0.50% in 2016. The number of patches, or areas of disconnected classes, shows a doubling of infrastructure patches between 1988 and 1998, but a decrease to three patches in 2016. The *Largest Patch Index* (LPI) details the percent of landscape covered by the largest patch of each class. *Edge Density*

compares the length of edges of each category divided by the total landscape area, allowing comparison to other regions. This reflects increasing development at a slowing rate through time, with the same values for both classes because the edge boundary is between the two defined classes. *Correlation Length* "gives the distance one might traverse while staying in any patch from a random starting point" (McGarigal 2000). The increasing correlation length for the infrastructure class continued from 1988 to 2007 and then stabilized to 2016; in contrast, the distance one could travel without leaving the undisturbed class decreased (Figure 10). Over the 28-year period, the correlation length for infrastructure increased by 6.08 km.

The *Class Area* and *Core Area* both quantify the expansion of infrastructure through time relative to the entire peninsula. The variation in the number of patches reflect the inconsistent growth of the field and recovery of some of the early roads which were then abandoned. Lastly, increasing correlation length over time reflects what is already shown in the class area metric that as infrastructure expands, so too does the distance one could travel within an infrastructure patch.

As discussed earlier, this study only compared developed and undeveloped categories. Because of this binary assessment, assessment of a land-cover class specific fragmentation could not be performed. Differences in the extent used in Wallace's fragmentation analysis, meant direct comparisons could not be made between those metrics based upon area. For instance, Wallace reported 5% (2012), but that was based upon a constrained area of just infrastructure and buffers.

This study assessed the total impact of infrastructure development on most of the Tazovsky Peninsula. The overall 0.5% of landscape disturbed by infrastructure is well below the 4% reported by Weller et al. (2002), who included pipelines as well as roads and facilities, and

used ~1 m aerial imagery. Khitun and Rebristaya (2002) reported that Bykova (1995) found a total landscape disturbance of the Yamburg field at 1.5% of the entire Tazovsky Peninsula. However, that study included a broader definition of impacts, including heavy track vehicle paths, dumping of garbage, temporary camps, and exploratory drilling and they did not show the boundary which was used and could have included a larger area to the south (Khitun and Rebristaya 2002). If this study were able to map these other impacts from the Landsat imagery, the percent of disturbed landscape would most likely be similar to the 1.5% from Bykova (1995). However, this study aligns more with Preston and Kim's (2016) study of oil infrastructure landscape fragmentation within the Williston Basin. Their study concluded that 0.4% of the entire basin was directly impacted by infrastructure (pads, wells, and roads).

Comparison to Wallace can be made on several metrics. In terms of mapped infrastructure extent, this study found a larger area of disturbance than Wallace (2012). In 2007, for instance, Wallace mapped 71.4 km^2 of infrastructure and this study found 92.1 km^2. This study had more undisturbed patches but fewer developed patches than Wallace (2012). Comparing 2007, he found 69 undeveloped and 17 developed patches while this study had 79 undisturbed and 4 infrastructure patches. These differences reflect slight changes in methodology, including using a seasonal NDVI$_{max}$ instead of one image per year, digitizing road centers and applying a uniform buffer, and digitization by a different user. However, the overall similarity in the magnitudes and trends supports the robustness and replicability of the approach.
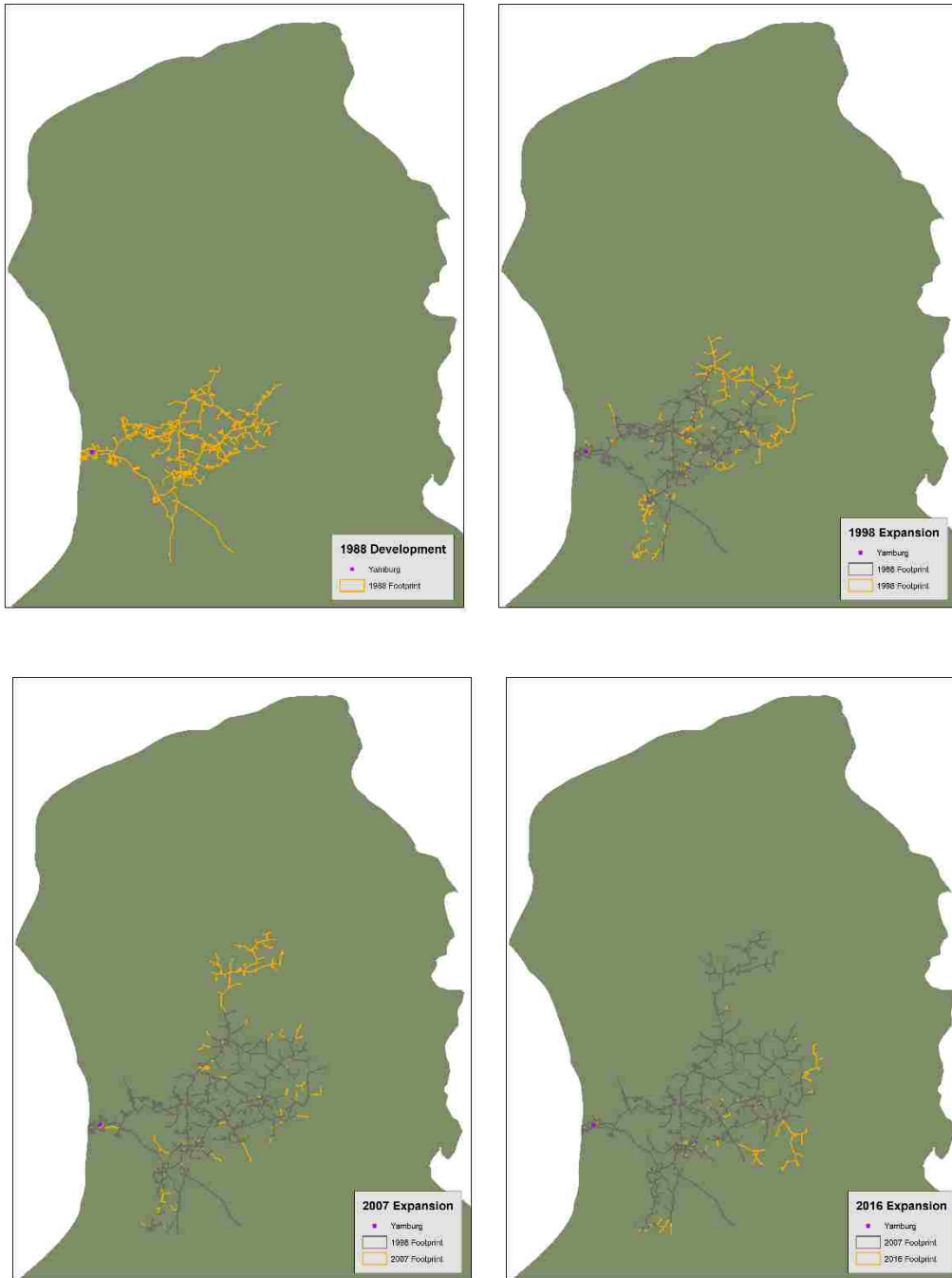
Figure 8. Maps showing the expansion of infrastructure across in the Tazovsky Peninsula from 1988 to 2016.
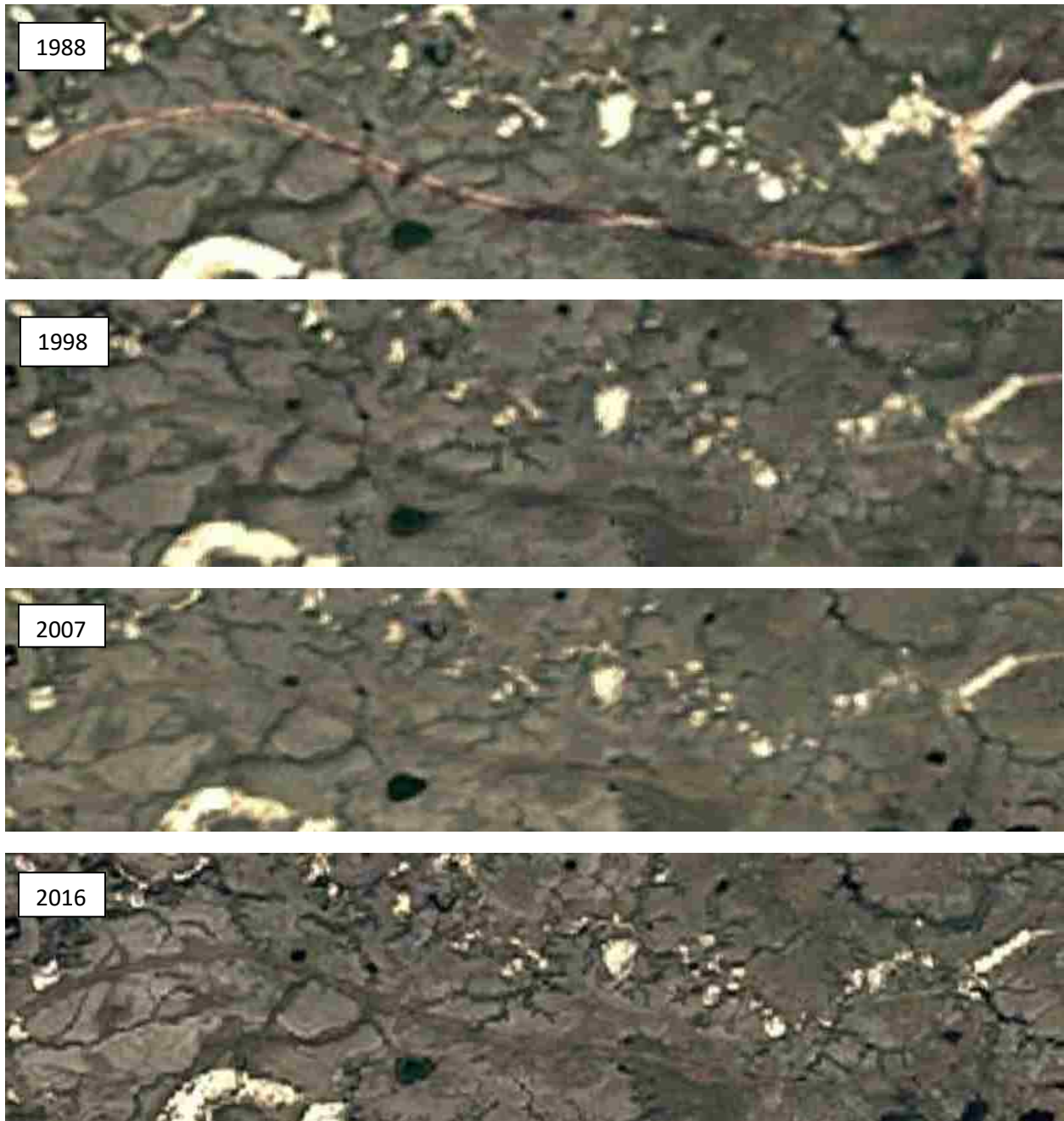
Figure 9. A road used during initial construction (1988), then abandoned (1998), and revegetated (2016). The scar is still visible on these true-color Landsat images. This 2016 Landsat 8 image is pan-sharpened to a 15 m resolution.

Fragmentation Metric	1983	1988	1998	2007	2016
Class Area (km²)					
Undeveloped	18722.79	18652.38	18638.79	18630.70	18629.14
Infrastructure	0.00	70.44	84.03	92.12	93.68
Landscape Percentage					
Undeveloped	100.00	99.62	99.55	99.51	99.50
Infrastructure	0.00	0.38	0.45	0.49	0.50
Patch Count					
Undeveloped	1	88	82	79	85
Infrastructure	0	3	6	4	3
Largest Patch Index (%)					
Undeveloped	100.00	97.16	95.90	95.68	95.68
Infrastructure	0.00	0.38	0.45	0.49	0.50
Edge Density					
Undeveloped	0.00	0.81	1.08	1.28	1.37
Infrastructure	0.00	0.81	1.08	1.28	1.37
Correlation Length (km)					
Undeveloped	55.28	54.79	54.67	54.64	54.65
Infrastructure	0.00	14.57	17.56	20.16	20.65

Table 5. Fragmentation metrics for each year based upon the digitized infrastructure. Core Area is the same as Class Area because only two categories were used.
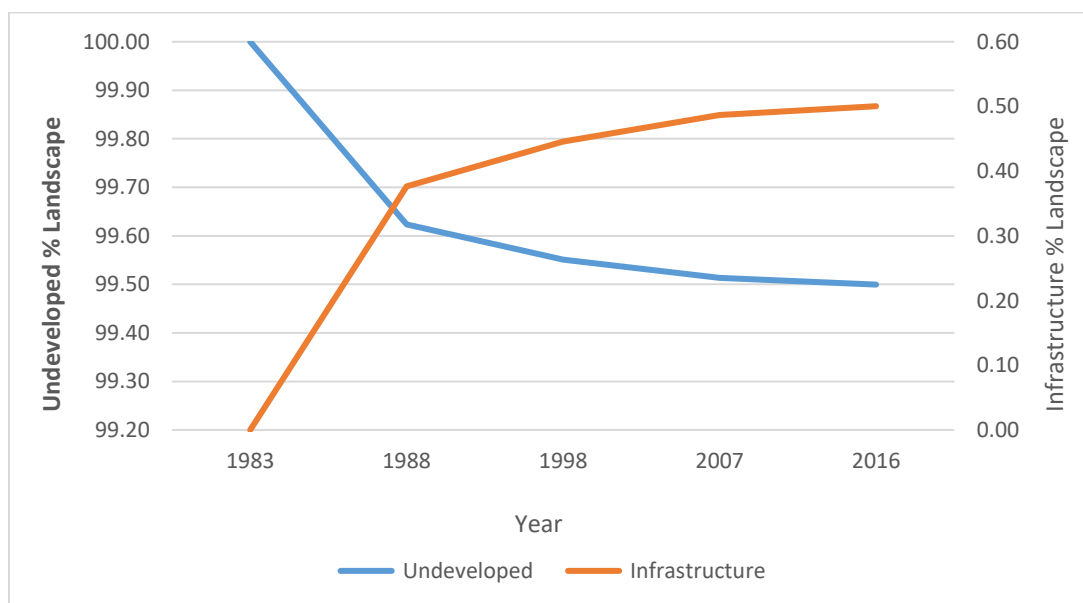
Figure 10. Percent of Landscape shifts of undeveloped and infrastructure between 1983 and 2016.
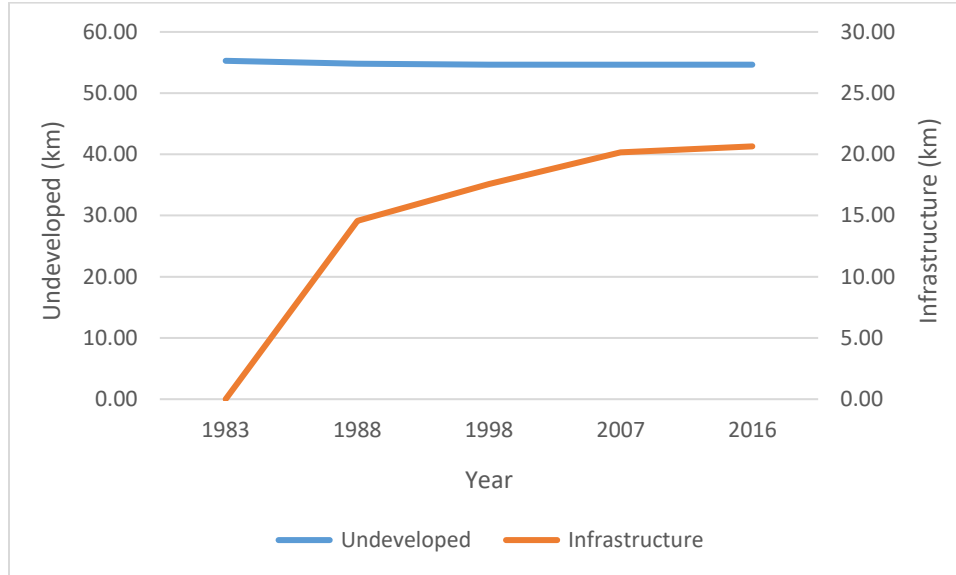
Figure 11. Change in Correlation Length for undeveloped and infrastructure between 1983 and 2016.

NDVI Analysis Results and Discussion

Analysis of the mean of the maximum NDVI values, $\overline{NDVI_{max}}$, within each buffer

(Figure 9) shows that all time slices have a similar pattern as distance increases from

infrastructure, with the lowest values within 30 meters of infrastructure, increasing to a slight

peak, then decreasing slowly to the farthest buffer. The values for 1988 begins low within 30 m,

steadily increasing out to 120 m and then stabilizing, followed by with a slight decrease to

600 m. Compared to its control areas, the $\overline{NDVI_{max}}$ values near infrastructure in 1988 remains

lower than those values. For the 1998, 2007, and 2016 time slices, the $\overline{NDVI_{max}}$ values increase

to the 60 and 90 m intervals but steadily decline past 120 m. The 1998, 2007, and 2016

$\overline{NDVI_{max}}$ curves lie between those for control areas 1 and 3 (Figure 9).

For all years, the Landsat $\overline{NDVI_{max}}$ shows that less green vegetation occupies the buffers closest to infrastructure but returns to background values with increasing distance. This trend aligns with the results found by Walker and Everett (1987) and Myers et al. (2006) of vegetation disturbance occurring closer to infrastructure and seeing a return to more natural land-cover as distance increases. Examination of the $\overline{NDVI_{max}}$ values from 1988 suggests that during initial field development, disturbance was prevalent. Photographs of the area (Figure 10) and the Landsat imagery, show that off-road and other vehicle tracks were very common during initial construction but less so once infrastructure was completed. Construction practices in Yamburg were not as carefully limited just to the boundaries of the infrastructure footprint as they are in Prudhoe Bay, Alaska, for example (Klene, pers. comm.), nor are efforts utilized to mitigate the spatial extent of disturbance as they are in some other fields.

Gradual recovery can be seen in 1998, 2007, and 2016 as $\overline{NDVI_{max}}$ values begin to increase within the buffers in comparison to the control sites. The lower $\overline{NDVI_{max}}$ values directly next to the roads and pads suggests that vegetation in immediate proximity to the infrastructure is less green because it is less healthy, there is less of it, or that water pooling along the infrastructure is suppressing the values. A combination of these factors is also possible. The cause of the highest values between 60 and 90 meters may be the result of increased lush vegetation due to higher moisture because of changes in hydrology and drainage which can extend for 10s to 100s of meters away from infrastructure, and/or fertilization effects from road dust (Walker and Everett 1987 and Myers et al. 2006). If regrowth was observed, due to the spatial and spectral limitations of Landsat imagery and lack of species-specific spectral signatures, it was not feasible to determine whether the new vegetation was native or invasive species.

The overall higher $\overline{NDVI_{max}}$ values in 2016 than in the other years (Figure 9) may be related to sensor differences between Landsat 5 and 8 (Li et al. 2013; Xu et al. 2014; Roy et al. 2016). Conversion and comparisons between these sensors is currently the focus of considerable effort in the research community (Roy et al. 2016).

When compared to Wallace (2012), the resulting NDVI curves have similar shaping though the values for this study are consistently higher due to the use of $\overline{NDVI_{max}}$ values from a seasonal stack of imagery and differences in image processing. Wallace (2012) used uncorrected imagery which may have larger pixel value inconsistencies between time slices than the L1T Top of Atmosphere (TOA) processed imagery used in this study (Yang and Lo 2000).

Change Analysis Results and Discussion

Changes in the categorized normalized $NDVI_{max}$ values (Table 4) between each time slice and the subsequent one were calculated using TerrSet's CROSSTAB module (Table 7 and Figure 12; complete results are in Appendix C). A summary of the changes within each buffer are discussed here**.**

Overall, most land-cover change occurred directly adjacent to the infrastructure or within 90 m. Across all years, 0 to 30 m experienced the most change in normalized $NDVI_{max}$. From 90 to 600 meters, the amount of change decreased and stabilized with increasing distance. For all years, the 150 to 600 m buffer had the highest and most consistent percentage of "no change". 1988-1998 and 2007-2016 had the highest positive change (increasing greenness) and some of the lowest negative change (decreased greenness). 1998-2007 had the lowest positive change and highest negative change.

Change between classes (Table 3) was primarily between infrastructure, sparse vegetation, and light green vegetation. Some of the largest negative change happens as undisturbed and sparse vegetation shifted to infrastructure. A large shift of positive change happens when pixels in infrastructure shift to a vegetated state. The largest shift of positive change was from sparse vegetation to light green vegetation. The largest shift of negative change was seen when light green vegetation downgrades to sparse vegetation.

The cross-tabulation results (Table 6 and Figure 13) lend insight into land-cover change within the buffers. Infrastructure expansion can be seen when any class changed to infrastructure, particularly with undisturbed and sparse vegetation. Class 0 was "non-infrastructure" land-cover not included in a buffer in a previous or subsequent time; any changes from that undisturbed category to infrastructure indicated new infrastructure expanding into land which was previously not near infrastructure. The reverse can also be said; when pixels move from infrastructure to non-infrastructure (class 0), abandonment had occurred. This claim was supported by visually assessing the appearance of roads now abandoned following construction (Figure 8) and revegetated, buried pipelines (Figure 14). Change from infrastructure to sparse vegetation indicates initial regrowth as the landscape moves from bare or disturbed to sparse vegetation. Negative shifts from light green vegetation to sparse vegetation may be explained by one of two things. First, results from Walker and Everett (1987) and Myers et al. (2006) on the impact of road dust may be acting in this region as well. With frequent traffic along major corridors, dust deposition can be heavy, covering and hindering growth or killing the vegetation. Secondly, small linear ponds of water could also be suppressing these NDVI values but this cannot be visually detected due to the spatial resolution of Landsat, although these are found throughout the area (Figure 15; Vilchek, 2000).
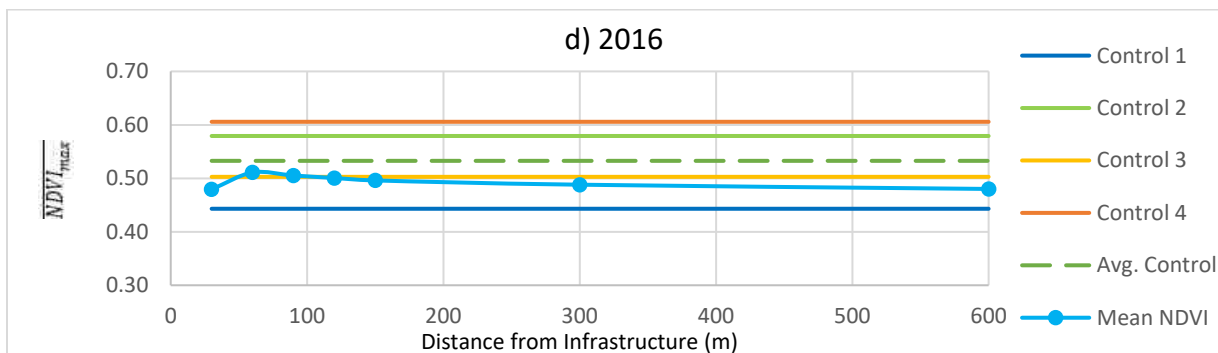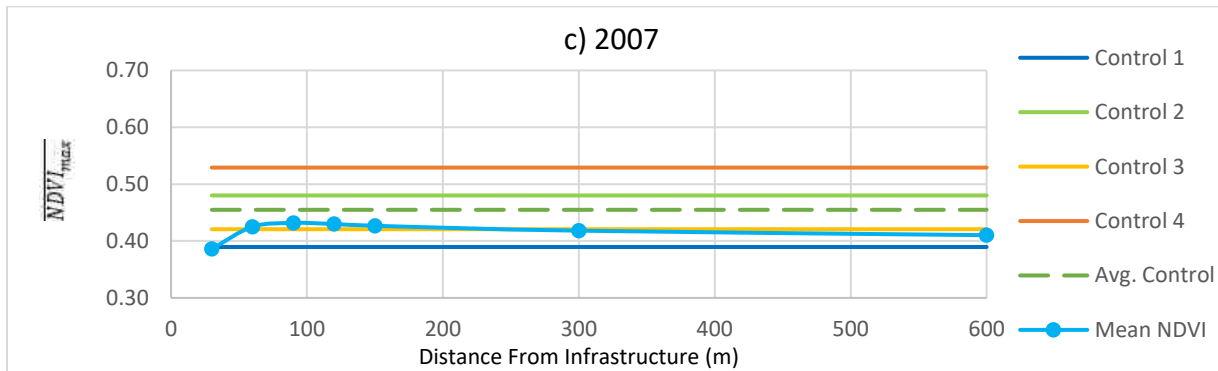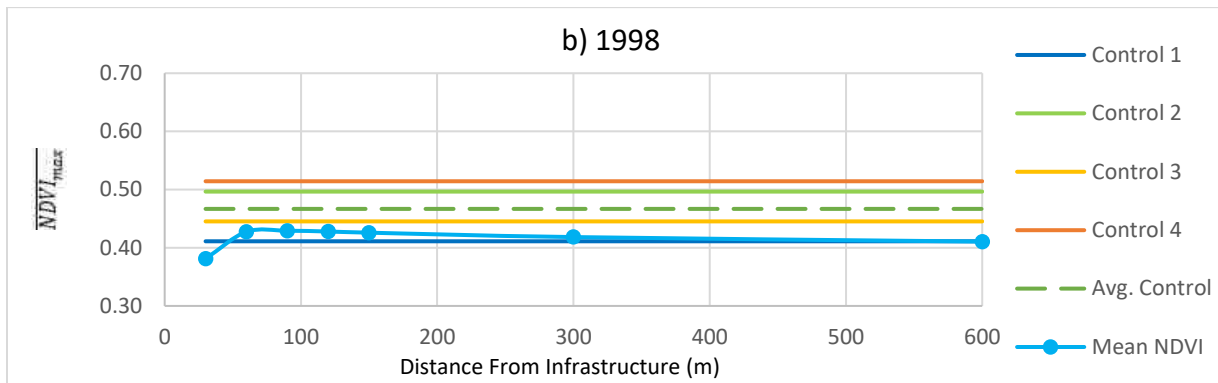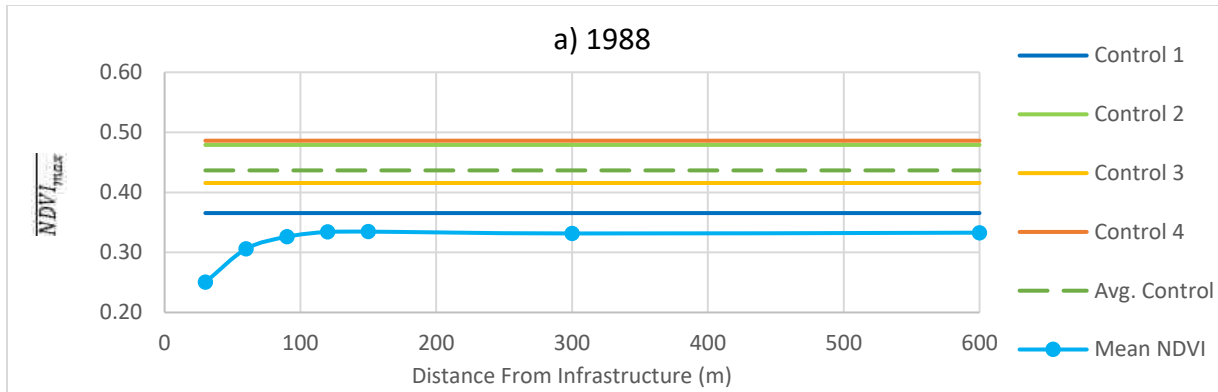
Figure 12. Mean maximum NDVI values within each buffer surrounding the digitized infrastructure for each year (a-d). Control areas 1-4 were selected to be progressively drier as shown in Figure 2.

Figure 13. Photographs show vehicle tracks cutting across undisturbed tundra (left) and the edge of a road with off-road vehicle tracks leading to the source of local sand used in road construction (right).

The road dust might also explain the positive shift from sparse vegetation to light green vegetation, as Walker and Everett (1987) and Myers et al. (2006) found that airborne dust can also cause a fertilization effect, increasing nutrients in the soil, allowing for enhanced vegetation growth.

Although change can be clearly seen between time slices, class-specific change, such as to or from water along roads, could not be seen because of the spatial resolution of the Landsat imagery. Additionally, because of this constraint, species-level assessment of plant greening or browning could not be performed. Studies within the region (Forbes 1997; Forbes 1999; Forbes and Jefferies 1999; Vilchek, 2000) found that during regrowth, non-native species or invasive species account for up to 40% of the plant community. Though these studies were not done specifically within the Yamburg field boundaries, it can be inferred that regrowth in this area has similar proportions of non-native plants.

Comparison of results with Wallace's study (2012) show that even though there were differences in calculation of the NDVI values (normalized $NDVI_{max}$ used in the present study vs single image NDVI by Wallace, as well as differences in the area used in subtraction between

layers) and more control areas utilized in this project, the general pattern is strikingly similar.

Wallace also found the most impact closest to infrastructure, decreasing with distance. The

shapes of his curves was slightly less consistent between time slices, and the shift of increasing

values within the buffers with time since the initial field construction was not as apparent. This

is consistent with what is expected from using the normalized $NDVI_{max}$ from the Landsat L1T

TOA product (Yang and Lo 2000) instead of the single images used in Wallace (2012).

Year	Buffer Distance	Positive %	Negative %	No Change %
1988 to 1998	0 to 30	28.20	16.23	55.57
	30 to 90	22.99	11.83	65.18
	90 to 150	14.98	8.98	76.04
	150 to 600	10.68	9.72	79.61
1998 to 2007	0 to 30	18.13	17.31	64.56
	30 to 90	15.23	13.25	71.52
	90 to 150	12.03	9.48	78.49
	150 to 600	9.83	10.21	79.97
2007 to 2016	0 to 30	24.45	9.28	66.28
	30 to 90	17.27	10.38	72.35
	90 to 150	9.15	12.31	78.54
	150 to 600	7.67	12.36	79.97

Table 6. Change in greenness category for each buffer surrounding the digitized infrastructure from one time slice to the next.
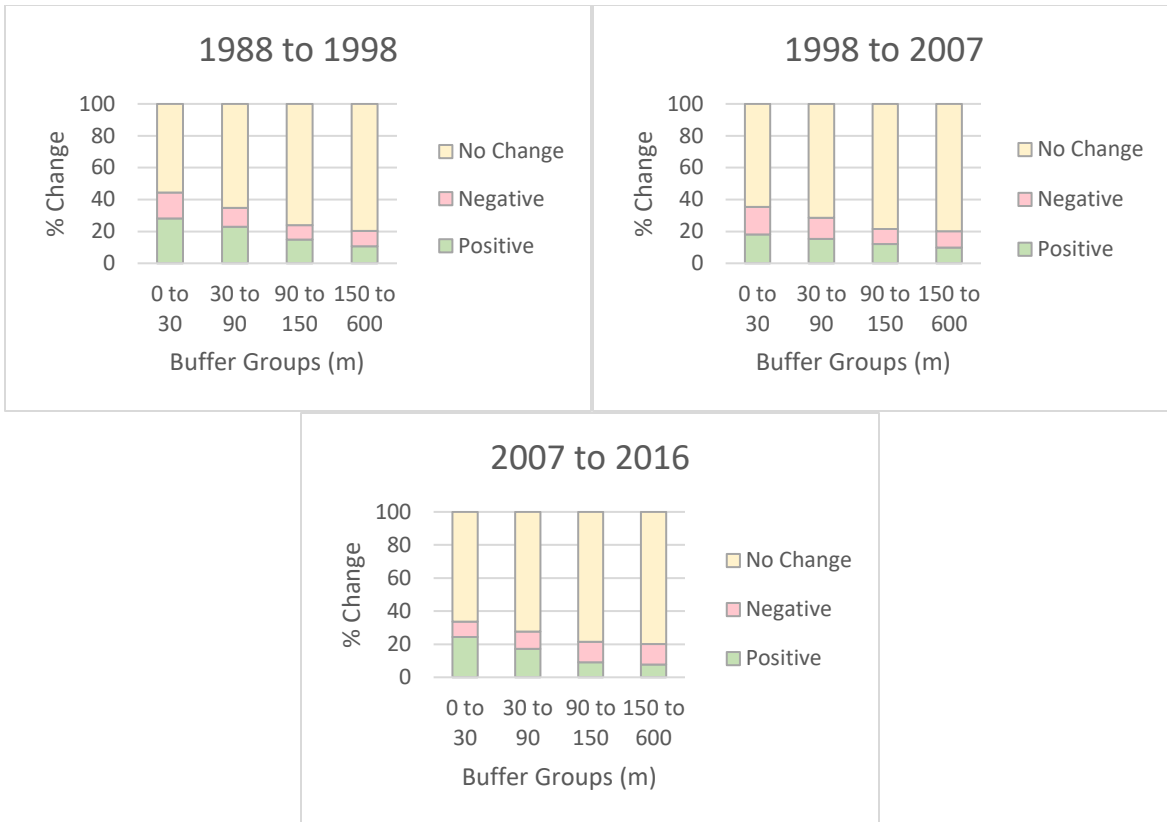
Figure 14. Change in greenness category (Table 6) for each buffer surrounding the digitized infrastructure from one time slice to the next.

Figure 15. A pipeline buried by locally sourced sand showing revegetation.

Figure 16. Small, linear features of pooling water adjacent to a road Pooling is caused by road construction altering the height of the permafrost table and resulting changes in hydrology.

Google Earth Engine

  Google Earth Engine provided a powerful entry point into land-cover analysis, specifically dealing with change over time. GEE can query and preprocess imagery with similar ability to traditional methods but much more quickly. Its ability to analyze stacks of images can provide researchers with a more robust dataset, such as in this study where instead of a single image from each year, the maximum value for each pixel was extracted from up to 29 images in minutes instead of hours as would have been necessary using traditional methods.

  However, GEE is still in development, and the platform has limitations. Though GEE has a large image library and continuously ingests imagery from data providers, many image collections are incomplete. Because of limited processing resources, the development team must prioritize more in-demand regions. While all regions have some data, for this study area only the Landsat top of atmosphere reflectance L1T collection (mid-level processed data) was available, a significant improvement over unprocessed, raw satellite images, but not as desirable for some applications as the unavailable, more accurate surface reflectance collection.

  GEE is primarily a raster-processing platform, and its ability to handle complex vector data has not been developed as extensively. The hand-digitized infrastructure footprint was a complex polygon that GEE could not properly display because it had more than the maximum allowed number of vertices in spring 2017. Because of this limitation, accurate zonal values could not be extracted within GEE, preventing the entire analysis process from being done within one software. Instead, ArcGIS, TerrSet, and FRAGSTATS were needed to handle the vector data analysis, change analysis, and landscape fragmentation analysis respectively.

Conclusions and Future Research

Conclusions

This study assessed the impacts of development on vegetation greenness across the Yamburg oil and gas field. Fragmentation analysis quantified total landscape disturbance and showed that the rate of fragmentation reflects the growth of the field. During initial field development, the infrastructure rapidly expanded and heavily fragmented the landscape. As production continued, both growth and fragmentation slowed. Analysis of nested buffers surrounding the infrastructure showed $\overline{NDVI_{max}}$ values within these buffers were lower closer to the infrastructure, with most of the impact within 150 m, and returned to nearly undisturbed values by 600 m away from infrastructure. All of the buffer values became more similar to background levels with increasing time from initial field construction. Change analysis was done (after normalizing to reduce the impacts of seasonality) by categorizing the normalized $NDVI_{max}$ values and cross tabulating these between time slices. This analysis showed disturbance and recovery as the field grew. Google Earth Engine served as an image repository and data manipulation resource which substantially improved these analyses compared to traditional methods. Conclusions made from this case study not only further our understanding on the impacts of climatic warming and infrastructure development in the Arctic, but also explore a new method for future remote sensing studies of land-cover change.

Future Research

This research presented methods for remote analysis of extraction infrastructure impacts on Arctic tundra. Though the extent and magnitude of impact could be observed and quantified, a land-cover classification based analysis would provide better assessment of the magnitude of

the various types of disturbance. Limiting factors included the spatial resolution of the Landsat data, a lack of previous land-cover mapping in the region, no access to existing maps of infrastructure, a lack of vector data manipulation tools within in Google Earth Engine, and little access to *in situ* validation data.

Although Landsat provides a long history of spatially and spectrally consistent imagery, the 30 m resolution limited the results. Higher resolution imagery would better describe the changes on the landscape, more types of disturbance could be seen, allowing for more detailed classifications, improved footprint digitization, land-cover accuracy, and change assessment. Currently existing Landsat imagery with additional corrections beyond the L1T TOA product used here were not yet ingested into GEE for this region. Future processing of imagery archives by USGS or other groups to systematically account for additional changes in sensor calibration and drift (Chander et al. 2009), BRDF correction (Buchhorn et al., 2016), differences in sensor design (Li et al. 2013) may be implemented and improve the reliability of the Landsat record for these types of time series analyses.

As mentioned earlier, due to the lack of high-resolution land-cover maps of the region, a binary categorization of developed and undeveloped was used for the fragmentation analysis. Access to land-cover maps would have facilitated more complex fragmentation analysis of impacts specific to each land-cover class. Having ground truth data within each buffer would have allowed for an accuracy assessment, and NDVI values could have been interpreted with more confidence, such as determining if pooling water was suppressing NDVI values, and hopefully improved accuracy.

Google Earth Engine (GEE) is a powerful entry point into efficient manipulation of large volumes of imagery. While it limited the vector data processing, presumably this will be

resolved soon. One alternative way to handle the current limitation of the KML file input would be to convert the buffers and footprints to rasters, allowing for more of the analyses to be implemented within GEE. The recent addition of shapefile support may also resolve the KML limitations.

Finally, landscape trajectory analysis, which uses changes in spectral signatures of groups of pixels in the study area to assess changes in landscape patterns over time. These work best with land-cover classifications finer than that used in this study but can provide, "rigorous, intuitive and highly interpretable description of interactions" of landscape change (Cushman and McMarigal 2007).

References

Agriculture and Agri-Food Canada; Government of Canada. "Agriculture and Agri-Food Canada (AAFC) - Home." Agriculture and Agri-Food Canada; Government of Canada. Accessed July 29, 2017.

Anderson, J. R. *A land use and land cover classification system for use with remote sensor data*. Vol. 964. United States Geological Survey, 1976.

Andren, H. "Effects of habitat fragmentation on birds and mammals in landscapes with different proportions of suitable habitat: a review." *Oikos* 71, no. 3 (1994): 355-366.

Arctic Council. "Impacts of a warming arctic: Arctic climate impact assessment." In Fourth Arctic Council Ministerial Meeting. 2004.

Bashkin, V. N., P. A. Barsukov, and A. K. Arabsky. "Specific Reaction of Biota to Environmental Pollution in Tundra Ecosystems." In: V. N. Bashkin *Biogeochemical Technologies for Managing Pollution in Polar Ecosystems*, pp. 73-85. Springer International Publishing, 2017.

Beck, P. and S. J. Goetz. "Satellite observations of high northern latitude vegetation productivity changes between 1982 and 2008: ecological variability and regional differences." *Environmental Research Letters* 6, no. 4 (2011): 045501.

Billings, W. D. "Constraints to plant growth, reproduction, and establishment in arctic environments." *Arctic and Alpine Research* 19, no. 4 (1987): 357-365.

Broich, M., M. C. Hansen, P. Potapov, B. Adusei, E. Lindquist, and S. V. Stehman. "Time-series analysis of multi-resolution optical imagery for quantifying forest cover loss in Sumatra and Kalimantan, Indonesia." *International Journal of Applied Earth Observation and Geoinformation* 13, no. 2 (2011): 277-291.

Brown, M. E., J. E. Pinzón, K. Didan, J. T. Morisette, and C. J. Tucker. "Evaluation of the consistency of long-term NDVI time series derived from AVHRR, SPOT-vegetation, SeaWiFS, MODIS, and Landsat ETM+ sensors." *IEEE Transactions on Geoscience and Remote Sensing* 44, no. 7 (2006): 1787-1793.

Buchhorn, M., M. K. Raynolds, and D. A. Walker. "Influence of BRDF on NDVI and biomass estimations of Alaska Arctic tundra." *Environmental Research Letters* 11, no. 12 (2016): 1-12. doi:10.1088/1748-9326/11/12/125002

Chander, G., B. L. Markham, D. L. Helder. "Summary of current radiometric calibration coefficients for Landsat MSS, TM, ETM+ and EO-1 ALI sensors." *Remote Sensing of Environment* 113, no. 5 (2009) 893–903. doi:10.1016/j.rse.2009.01.007

Chapin, F. S. "Direct and indirect effects of temperature on arctic plants." *Polar Biology* 2, no. 1 (1983): 47-52.

Cihlar, J., I. Tcherednichenko, R. Latifovic, Z. Li, and J. Chen. "Impact of variable atmospheric water vapor content on AVHRR data corrections over land." *IEEE Transactions on Geoscience and Remote Sensing* 39, no. 1 (2001): 173-180.

Cushman, S. A., and D. O. Wallin. "Rates and patterns of landscape change in the Central Sikhote-alin Mountains, Russian Far East." *Landscape Ecology* 15, no. 7 (2000): 643-659.

Cushman S.A., and K. McGarigal. (2007). Multivariate Landscape Trajectory Analysis. In: Bissonette J.A., Storch I. (eds). *Temporal Dimensions of Landscape Ecology*. Springer, Boston, MA: 119 – 140.

Dong, J., X. Xiao, M. A. Menarguez, G. Zhang, Y. Qin, D. Thau, C. Biradar, and B. Moore. "Mapping paddy rice planting area in northeastern Asia with Landsat 8 images, phenology-based algorithm and Google Earth Engine." *Remote Sensing of Environment* 185 (2016): 142-154.

Eastman, J. R. "TerrSet: Geospatial Monitoring and Modeling Software." *Clark Labs, Clark University* (2015).

Fahrig, L. "Relative effects of habitat loss and fragmentation on population extinction." *The Journal of Wildlife Management* 61, no. 3 (1997): 603-610.

Forbes, B. C. "Tundra disturbance studies IV. Species establishment on anthropogenic primary surfaces, Yamal peninsula, northwest Siberia, Russia." *Polar Geography* 21:2 (1997): 79-100.

Fraser, R. H., I. Olthof, M. Carrière, A. Deschamps, and D. Pouliot. "Detecting long-term changes to vegetation in northern Canada using the Landsat satellite image archive." *Environmental Research Letters* 6, no. 4 (2011): 045502.

French, H. M. *The Periglacial Environment*. John Wiley & Sons, 2013.

Fuller, R. M., G. B. Groom, and A. R. Jones. "Land cover map of Great Britain. An automated classification of Landsat Thematic Mapper data." *Photogrammetric Engineering and Remote Sensing* 60, no. 5 (1994).

Gazprom Dobycha Yamburg. (2016). Informational and Promotional Materials. Yamburg, Russia.

Goetz, S. J., A. G. Bunn, G. J. Fiske, and R. A. Houghton. "Satellite-observed photosynthetic trends across boreal North America associated with climate and fire disturbance." *Proceedings of the National Academy of Sciences of the United States of America* 102, no. 38 (2005): 13521-13525.

Goetz, S. J., G. J. Fiske, and A. G. Bunn. "Using satellite time-series data sets to analyze fire disturbance and forest recovery across Canada." *Remote Sensing of Environment* 101, no. 3 (2006): 352-365.

Gong, P., J. Wang, L. Yu, Y. Zhao, Y. Zhao, L. Liang, Z. Niu et al. "Finer resolution observation and monitoring of global land cover: First mapping results with Landsat TM and ETM+ data." *International Journal of Remote Sensing* 34, no. 7 (2013): 2607-2654.

Gorelick, N., M. Hancher, M. Dixon, S. Ilyushchenko, D. Thau, and R. Moore. "Google Earth Engine: Planetary-scale geospatial analysis for everyone." *Remote Sensing of Environment*, 2017.

Harrison, S., and E. Bruna. "Habitat fragmentation and large-scale conservation: What do we know for sure?" *Ecography* 22, no. 3 (1999): 225-232.

Holben, B. N. "Characteristics of maximum-value composite images from temporal AVHRR data." *International Journal of Remote Sensing* 7, no. 11 (1986): 1417-1434.

Huang, C., S. N. Goward, J. G. Masek, F. Gao, E. F. Vermote, N. Thomas, K. Schleeweis et al. "Development of time series stacks of Landsat images for reconstructing forest disturbance history." *International Journal of Digital Earth* 2, no. 3 (2009): 195-218.

Johansen, K., S. Phinn, and M. Taylor. "Mapping woody vegetation clearing in Queensland, Australia from Landsat imagery using the Google Earth Engine." *Remote Sensing Applications: Society and Environment* 1 (2015): 36-49.

Johnston, R. M., and M. M. Barson. "Remote sensing of Australian wetlands: An evaluation of Landsat TM data for inventory and classification." *Marine and Freshwater Research* 44, no. 2 (1993): 235-252.

Karlsen, S. R., A. Tolvanen, E. Kubin, J. Poikolainen, K. Arild Høgda, B. Johansen, F. S. Danks, P. Aspholm, F. Emil Wielgolaski, and O. Makarova. "MODIS-NDVI-based mapping of the length of the growing season in northern Fennoscandia." *International Journal of Applied Earth Observation and Geoinformation* 10, no. 3 (2008): 253-266.

Kawamura, K., T. Akiyama, H. Yokota, M. Tsutsumi, T. Yasuda, O. Watanabe, and S. Wang. "Comparing MODIS vegetation indices with AVHRR NDVI for monitoring the forage quantity and quality in Inner Mongolia grassland, China." *Grassland Science* 51, no. 1 (2005): 33-40.

Khitun, O., and O. Rebristaya. "Anthropogenic impacts on habitat structure and species richness in the West Siberian Arctic." (2002). In: Watson, A.E.; Alessa, L. Sproull, J., comps. *Wilderness in the Circumpolar North: Searching for compatibility in ecological, traditional, and ecotourism values*. 2001 May 15-16; Anchorage, AK. Proceedings RMRS-P-26. Ogden, UT: U.S. Department of Agriculture, Forest Service, Rocky Mountain Research Station. p. 85-95.

Klemas, V. V. "Remote sensing of landscape-level coastal environmental indicators." *Environmental Management* 27, no. 1 (2001): 47-57.

Kontgis, C., A. Schneider, and M. Ozdogan. "Mapping rice paddy extent and intensification in the Vietnamese Mekong River Delta with dense time stacks of Landsat data." *Remote Sensing of Environment* 169 (2015): 255-269.

Lanorte, A., R. Lasaponara, M. Lovallo, and L. Telesca. "Fisher–Shannon information plane analysis of SPOT/VEGETATION Normalized Difference Vegetation Index (NDVI) time series to characterize vegetation recovery after fire disturbance." *International Journal of Applied Earth Observation and Geoinformation* 26 (2014): 441-446.

Larsen, P. H., S. Goldsmith, O. Smith, M. L. Wilson, K. Strzepek, P. Chinowsky, and B. Saylor. "Estimating future costs for Alaska public infrastructure at risk from climate change." *Global Environmental Change* 18, no. 3 (2008): 442-457.

Li, P., L. Jiang, and Z. Feng. "Cross-comparison of vegetation indices derived from Landsat-7 Enhanced Thematic Mapper plus (ETM+) and Landsat-8 Operational Land Imager (OLI) sensors." *Remote Sensing* 6, no. 1 (2013): 310-329.

Martínez, B., and M. A. Gilabert. "Vegetation dynamics from NDVI time series analysis using the wavelet transform." *Remote Sensing of Environment* 113, no. 9 (2009): 1823-1842.

Masek, J. G., C. Huang, R.Wolfe, W. Cohen, F. Hall, J. Kutler, and P. Nelson. "North American forest disturbance mapped from a decadal Landsat record." *Remote Sensing of Environment* 112, no. 6 (2008): 2914-2926.

Mazhitova, G., N. Karstkarel, N. Oberman, V. Romanovsky, and P. Kuhry. "Permafrost and infrastructure in the Usa Basin (Northeast European Russia): Possible impacts of global warming." *AMBIO: A Journal of the Human Environment* 33, no. 6 (2004): 289-294.

McGarigal, K., S. Cushman, S. G. Stafford. *Multivariate Statistics for Wildlife and Ecology Research*. Vol. 279. New York: Springer, 2000.

McGarigal, K., SA Cushman, and E Ene. 2012. FRAGSTATS v4: Spatial Pattern Analysis Program for Categorical and Continuous Maps. Computer software program produced by the authors at the University of Massachusetts, Amherst. Available at the following web site: http://www.umass.edu/landeco/research/fragstats/fragstats.html

Moore, M. M., and M. E. Bauer. "Classification of forest vegetation in north-central Minnesota using Landsat Multispectral Scanner and Thematic Mapper data." *Forest Science* 36, no. 2 (1990): 330-342.

Morren, C. *Fleurs Éphémères*. Perichon, 1843.

Muller, S. W. "*Permafrost or Permanently Frozen Ground and Related Engineering Problems*." Special Report, Strategic Engineering Study no. 62. Intelligence Branch, Office of the Chief of Engineers (1943).

Myers-Smith, I. H., B. K. Arnesen, R. M. Thompson, and F. S. Chapin III. "Cumulative impacts on Alaskan arctic tundra of a quarter century of road dust." *Ecoscience* 13, no. 4 (2006): 503-510.

Myneni, R. B., C. D. Keeling, C. J. Tucker, G. Asrar, and R. R. Nemani. "Increased plant growth in the northern high latitudes from 1981 to 1991." *Nature* 386, no. 6626 (1997): 698.

National Research Council. *Cumulative Environmental Effects of Oil and Gas Activities on Alaska's North Slope*. National Academies Press, 2003.

Narasimhan, R., and D. Stow. "Daily MODIS products for analyzing early season vegetation dynamics across the North Slope of Alaska." *Remote sensing of Environment* 114, no. 6 (2010): 1251-1262.

Nelson, F. E., O. A. Anisimov, and N. I. Shiklomanov. "Subsidence risk from thawing permafrost." *Nature* 410, no. 6831 (2001): 889-890.

Nelson, R. F., R. S. Latty, and G. Mott. "Classifying northern forests using Thematic Mapper simulator data." *Photogrammetric Engineering and Remote Sensing* 50, n. 5 (1984): 607 – 617.

Patel, N. N., E. Angiuli, P. Gamba, A. Gaughan, G. Lisini, F. R. Stevens, A. J. Tatem, and G. Trianni. "Multitemporal settlement and population mapping from Landsat using Google Earth Engine." *International Journal of Applied Earth Observation and Geoinformation* 35 Part B (2015): 199-208.

"Population." *YamalStat*. Accessed November 07, 2016.
    http://yamalstat.gks.ru/wps/wcm/connect/rosstat_ts/yamalstat/ru/statistics/population/

Preston, T. M., and K. Kim. "Land cover changes associated with recent energy development in
    the Williston Basin; Northern Great Plains, USA*." Science of the Total Environment*, vol.
    566-567 (2016): 1511–1518.

Raynolds, M. K., D. A. Walker, K. J. Ambrosius, J. Brown, K. R. Everett, M. Kanevskiy, G. P.
    Kofinas, V. E. Romanovsky, Y. Shur, and P. J. Webber. "Cumulative geoecological
    effects of 62 years of infrastructure and climate change in ice rich permafrost landscapes,
    Prudhoe Bay Oilfield, Alaska." *Global Change Biology* 20, no. 4 (2014): 1211-1224.

Raynolds, M. K., J. C. Comiso, D. A. Walker, and D. Verbyla. "Relationship between satellite-
    derived land surface temperatures, arctic vegetation types, and NDVI." *Remote Sensing
    of Environment* 112, no. 4 (2008): 1884-1894.

Reed, B. C., M. D. Schwartz, and X. Xiao. "Remote sensing phenology." In *Phenology of
    Ecosystem Processes*, pp. 231-246. Springer New York, 2009.

Reese, H.M., T. M. Lillesand, D. E. Nagel, J. S. Stewart, R. A. Goldmann, T. E. Simmons, J. W.
    Chipman, and P. A. Tessar. "Statewide land cover derived from multiseasonal Landsat
    TM data: a retrospective of the WISCLAND project." *Remote Sensing of Environment*
    82, no. 2 (2002): 224-237.

Rees, W. G., and A. P. Kapitsa. "Industrial pollution in the Kol'skiy Poluostrov, Russia." *Polar
    Record* 30, no. 174 (1994): 181-188.

Rees, W. G., and M. Williams. "Monitoring changes in land cover induced by atmospheric
    pollution in the Kola Peninsula, Russia, using Landsat-MSS data." *International Journal
    of Remote Sensing* 18, no. 8 (1997): 1703-1723.

Rees, W. G., M. Williams, and P. Vitebsky. "Mapping land cover change in a reindeer herding
    area of the Russian Arctic using Landsat TM and ETM+ imagery and indigenous
    knowledge." *Remote Sensing of Environment* 85, no. 4 (2003): 441-452.

Robin, J., R. Dubayah, E. Sparrow, and E. Levine. "Monitoring start of season in Alaska with
    GLOBE, AVHRR, and MODIS data." *Journal of Geophysical Research:
    Biogeosciences* 113, no. G1 (2008).

Röder, A., Th Udelhoven, J. Hill, G. Del Barrio, and G. Tsiourlis. "Trend analysis of Landsat-
    TM and-ETM+ imagery to monitor grazing impact in a rangeland ecosystem in Northern
    Greece." *Remote Sensing of Environment* 112, no. 6 (2008): 2863-2875.

Rouse Jr, JW, R.H. Haas, J.A. Schell, and D.W. Deering. "Monitoring vegetation systems in the Great Plains with ERTS." *Proceedings of the Third Earth Resources Technology Satellite- 1 Symposium* (1974): 309 – 317.

Roy, D. P., V. Kovalskyy, H. K. Zhang, E. F. Vermote, L. Yan, S. S. Kumar, and A. Egorov. "Characterization of Landsat-7 to Landsat-8 reflective wavelength and normalized difference vegetation index continuity." *Remote Sensing of Environment* 185 (2016): 57-70.

Saich, P., W. G. Rees, and M. Borgeaud. "Detecting pollution damage to forests in the Kola Peninsula using the ERS SAR." *Remote Sensing of Environment* 75, no. 1 (2001): 22-28.

Schneider, M. F. "Habitat loss, fragmentation and predator impact: spatial implications for prey conservation." *Journal of Applied Ecology* 38, no. 4 (2001): 720-735.

Schroeder, T. A., M. A. Wulder, S. P. Healey, and G. G. Moisen. "Mapping wildfire and clearcut harvest disturbances in boreal forests with Landsat time series data." *Remote Sensing of Environment* 115, no. 6 (2011): 1421-1433.

Schwartz, M. D. "Green-wave phenology." *Nature* 394, no. 6696 (1998): 839-840.

Seligman, B. J. "Long-term variability of pipeline-permafrost interactions in north-west Siberia." *Permafrost and Periglacial Processes* 11, no. 1 (2000): 5-22.

Shiklomanov, N. I., D. A. Streletskiy, T. B. Swales, and V. A. Kokorev. "Climate Change and Stability of Urban Infrastructure in Russian Permafrost Regions: Prognostic Assessment based on GCM Climate Projections." *Geographical Review* 107, no. 1 (2017): 125-142.

Southworth, J., Darla M., and H. Nagendra. "Land cover change and landscape fragmentation—comparing the utility of continuous and discrete analyses for a western Honduras region." *Agriculture, Ecosystems & Environment* 101, no. 2 (2004): 185-205.

Stueve, K. M., I. W. Housman, P. L. Zimmerman, M. D. Nelson, J. B. Webb, C. H. Perry, R.A. Chastain et al. "Snow-covered Landsat time series stacks improve automated disturbance mapping accuracy in forested landscapes." *Remote Sensing of Environment* 115, no. 12 (2011): 3203-3219.

Toutoubalina, O. V., and W. G. Rees. "Remote sensing of industrial impact on Arctic vegetation around Noril'sk, northern Siberia: Preliminary results." *International Journal of Remote Sensing* 20, no. 15-16 (1999): 2979-2990.

Trianni, G., E. Angiuli, G. Lisini, and P. Gamba. "Human settlements from Landsat data using Google Earth Engine." In *Geoscience and Remote Sensing Symposium (IGARSS), 2014 IEEE International*, pp. 1473-1476. IEEE, 2014.

Turner, M. G. "Landscape ecology: The effect of pattern on process." *Annual Review of Ecology and Systematics* 20, no. 1 (1989): 171-197.

Viedma, O., J. Meliá, D. Segarra, and J. García-Haro. "Modeling rates of ecosystem recovery after fires by using Landsat TM data." *Remote Sensing of Environment* 61, no. 3 (1997): 383-398.

Vilchek, G. "Environmental impact of oil and gas development." In *The Physical Geography of Northern Eurasia*, edited by M. Shahgedanova, Oxford University Press, 2002, pp. 463-475.

Walker, D. A. "Disturbance and recovery of arctic Alaskan vegetation." In *Landscape function and disturbance in Arctic tundra*, J.F. Raynolds and J.D. Tenhunen (eds.). Springer Berlin Heidelberg, 1996 pp. 35-71.

Walker, D. A., and K. R. Everett. "Road dust and its environmental impact on Alaskan taiga and tundra." *Arctic and Alpine Research* 19, no. 4 (1987): 479-489.

Walker, D. A., P. J. Webber, Emily F. Binnian, K. R. Everett, N. D. Lederer, E. A. Nordstrand, and M. D. Walker. "Cumulative impacts of oil fields on northern Alaskan landscapes." *Science* 238, no. 4828 (1987): 757-761.

Walker, D. A., M. K. Raynolds, M. Buchhorn, and J. L. Peirce. "Landscape and permafrost change in the Prudhoe Bay Oilfield, Alaska." *Alaska Geobotany Center, University of Alaska, AGC Publication* (2014): 14-01.

Walker, D. A., and W. Acevedo. *Vegetation and a LANDSAT-derived land cover map of the Beechey Point Quadrangle, Arctic Coastal Plain, Alaska*. CRREL Report 87 -5. Hanover, NH: U.S. Army Cold Regions Research and Engineering Laboratory, 1987.

Walker, D. A., W. A. Gould, H. A. Maier, and M. K. Raynolds. "The Circumpolar Arctic Vegetation Map: AVHRR-derived base maps, environmental controls, and integrated mapping procedures." *International Journal of Remote Sensing* 23, no. 21 (2002): 4551-4570.

Wallace, J. S., "Using Landsat Imagery to Evaluate Landscape-level Impacts of Natural Gas Field Development: Tazovsky Peninsula, Russia, 1984-2007" Master's thesis, University of Montana, 2012.

Weier, J., and D. Herring. "Measuring Vegetation (NDVI & EVI): Feature Articles." *NASA*. 2000. https://earthobservatory.nasa.gov/Features/MeasuringVegetation/

Weller, C. *Fragmenting Our Lands: The Ecological Footprint from Oil and Gas Development*. Wilderness Society, 2002: 2 - 20.

Xu, D., and X. Guo. "Compare NDVI extracted from Landsat 8 imagery with that from Landsat 7 imagery." *American Journal of Remote Sensing* 2, no. 2 (2014): 10-4.

Yakushev, V. S., and E. M. Chuvilin. "Natural gas and gas hydrate accumulations within permafrost in Russia." *Cold Regions Science and Technology* 31, no. 3 (2000): 189-197.

"Yamalo-Nenets-autonomous District"." *Finland Chamber of Commerce*. Accessed November 07, 2016. http://kauppakamari.fi/wp-content/uploads/2013/03/Yamalo-Nenets-autonomous-district.pdf

"Yamalo-Nenets Autonomous Region, Russia." *Russian Cities and Regions Guide Main Page*. Accessed December 12, 2016. http://russiatrek.org/yamalo-nenets-okrug.

Yang, X., and C. P. Lo. "Relative radiometric normalization performance for change detection from multi-date satellite images." *Photogrammetric Engineering and Remote Sensing* 66, no. 8 (2000): 967-980.

Zeng, H., G. Jia, and H. Epstein. "Recent changes in phenology over the northern high latitudes detected from multi-satellite data." *Environmental Research Letters* 6, no. 4 (2011): 045508.

Zhou, L., C. J. Tucker, R. K. Kaufmann, D. Slayback, N. V. Shabanov, and R. B. Myneni. "Variations in northern vegetation activity inferred from satellite data of vegetation index during 1981 to 1999." *Journal of Geophysical Research: Atmospheres* 106, no. D17 (2001): 20069-20083.

Appendices

1988 Mean NDVI Values						
Distance (m)	Mean NDVI	Control 1	Control 2	Control 3	Control 4	Avg. Control
30	0.25	0.37	0.48	0.42	0.49	0.44
60	0.31	0.37	0.48	0.42	0.49	0.44
90	0.33	0.37	0.48	0.42	0.49	0.44
120	0.33	0.37	0.48	0.42	0.49	0.44
150	0.33	0.37	0.48	0.42	0.49	0.44
300	0.33	0.37	0.48	0.42	0.49	0.44
600	0.33	0.37	0.48	0.42	0.49	0.44

1998 Mean NDVI Values						
Distance (m)	Mean NDVI	Control 1	Control 2	Control 3	Control 4	Avg. Control
30	0.38	0.41	0.50	0.45	0.51	0.47
60	0.43	0.41	0.50	0.45	0.51	0.47
90	0.43	0.41	0.50	0.45	0.51	0.47
120	0.43	0.41	0.50	0.45	0.51	0.47
150	0.43	0.41	0.50	0.45	0.51	0.47
300	0.42	0.41	0.50	0.45	0.51	0.47
600	0.41	0.41	0.50	0.45	0.51	0.47

2007 Mean NDVI Values						
Distance (m)	Mean NDVI	Control 1	Control 2	Control 3	Control 4	Avg. Control
30	0.39	0.39	0.48	0.42	0.53	0.45
60	0.43	0.39	0.48	0.42	0.53	0.45
90	0.43	0.39	0.48	0.42	0.53	0.45
120	0.43	0.39	0.48	0.42	0.53	0.45
150	0.43	0.39	0.48	0.42	0.53	0.45
300	0.42	0.39	0.48	0.42	0.53	0.45
600	0.41	0.39	0.48	0.42	0.53	0.45

2016 Mean NDVI Values						
Distance (m)	Mean NDVI	Control 1	Control 2	Control 3	Control 4	Avg. Control
30	0.48	0.44	0.58	0.50	0.61	0.53
60	0.51	0.44	0.58	0.50	0.61	0.53
90	0.51	0.44	0.58	0.50	0.61	0.53
120	0.50	0.44	0.58	0.50	0.61	0.53
150	0.50	0.44	0.58	0.50	0.61	0.53
300	0.49	0.44	0.58	0.50	0.61	0.53
600	0.48	0.44	0.58	0.50	0.61	0.53

Appendix A. Mean NDVI values extracted from each buffer and control area.
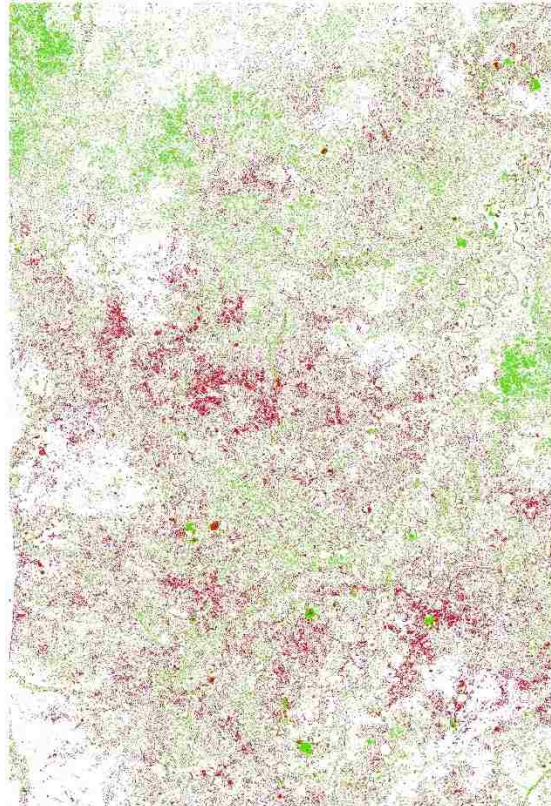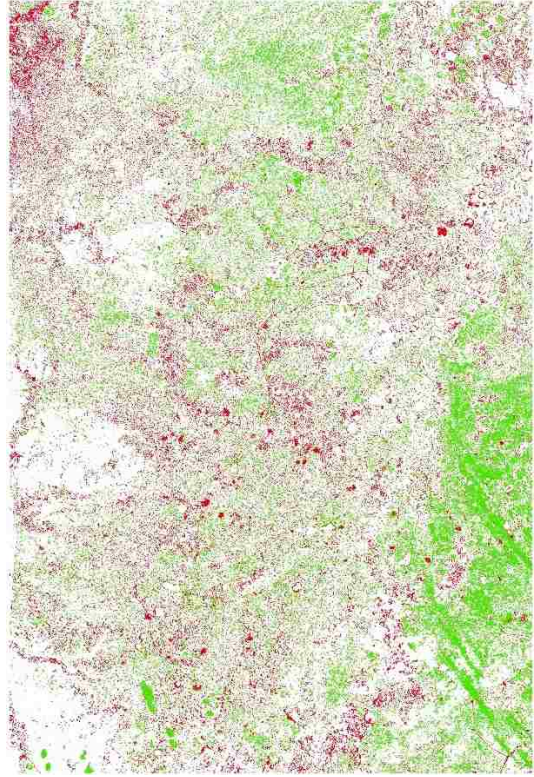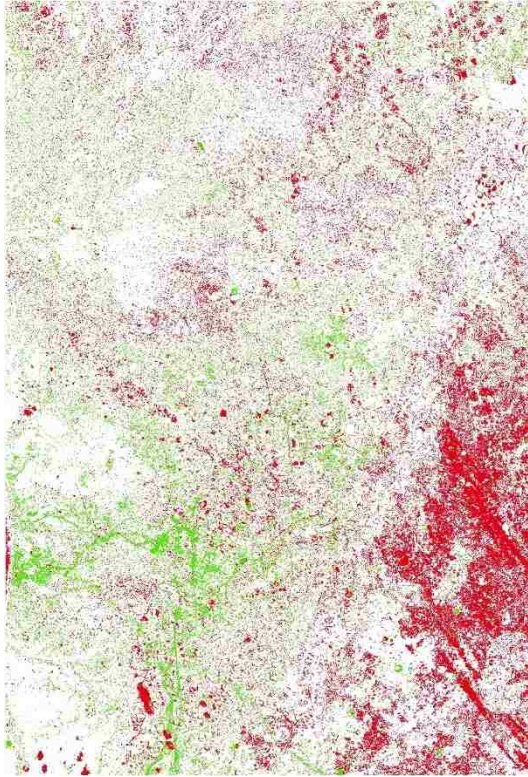
Appendix B. Reclassified cross tabulation outputs. 1988-1998 (top left), 1998-2007 (top right), and 2007-2016 (bottom middle).

2007 2016 0 to 30m

Category	2007 0	1	2	3	4	5	Total
0	10106082	6	1600	1889	1176	45	10110798
1	7	144	107	8	0	0	266
2	1332	62	5113	794	45	2	7348
3	5682	9	9778	21961	4709	7	42146
4	2230	0	735	6484	11480	255	21184
5	56	0	2	14	292	146	510
Total	10115389	221	17335	31150	17702	455	10182252

2007 2016 30 to 90m

Category	2007 0	1	2	3	4	5	Total
0	9964113	126	2673	5094	3468	135	9975609
1	197	1137	631	24	1	0	1990
2	1889	334	8426	1555	115	3	12322
3	14665	50	16338	65632	18064	22	114771
4	8081	4	1302	17234	47868	867	75356
5	278	0	6	62	1057	801	2204
Total	9989223	1651	29376	89601	70573	1828	10182252

2007 2016 90 to 150m

Category	2007 0	1	2	3	4	5	Total
0	9976212	289	1629	5164	4128	175	9987597
1	449	2997	1123	29	0	0	4598
2	1015	582	4513	1145	92	0	7347
3	13138	73	6429	64490	21358	15	105503
4	9750	16	304	10365	52749	956	74140
5	417	0	4	41	1218	1387	3067
Total	10000981	3957	14002	81234	79545	2533	10182252

2007 2016 150 to 600m

Category	2007 0	1	2	3	4	5	Total
0	9238790	1487	4369	18011	15365	847	9278869
1	3121	36906	8510	193	10	0	48740
2	5082	5417	28929	5928	458	3	45817
3	49410	553	26016	284717	90929	94	451719
4	46586	188	1658	39138	239041	5438	332049
5	3116	41	58	340	9242	12261	25058
Total	9346105	44592	69540	348327	355045	18643	10182252

1988 2007 0 to 30m

Category	1998 0	1	2	3	4	5	Total
0	10106050	71	3555	2909	2678	126	10115389
1	52	97	69	3	0	0	221
2	6844	118	7937	2336	100	0	17335
3	7937	18	5445	14030	3716	4	31150
4	4955	2	554	4207	7695	289	17702
5	123	0	8	26	156	142	455
Total	10125961	306	17568	23511	14345	561	10182252

1988 2007 30 to 90m

Category	1998 0	1	2	3	4	5	Total
0	9969867	410	4886	6525	7076	459	9989223
1	330	756	528	36	1	0	1651
2	9738	546	14202	4586	304	0	29376
3	20520	68	11528	45084	12365	36	89601
4	19414	5	1368	14416	34237	1133	70573
5	490	1	18	55	526	738	1828
Total	10020359	1786	32530	70702	54509	2366	10182252

1988 2007 90 to 150m

Category	1998 0	1	2	3	4	5	Total
0	9981286	665	3185	7327	7893	625	10000981
1	719	1947	1226	65	0	0	3957
2	3643	813	6894	2479	173	0	14002
3	19037	78	6405	45053	10641	20	81234
4	25695	18	722	13724	38141	1245	79545
5	828	0	8	30	535	1132	2533
Total	10031208	3521	18440	68678	57383	3022	10182252

1988 2007 150 to 600m

Category	1998 0	1	2	3	4	5	Total
0	9284236	2823	9846	22970	23528	2702	9346105
1	5555	26168	11966	880	23	0	44592
2	11775	6271	37655	12900	907	32	69540
3	71462	336	21267	208373	46758	131	348327
4	115400	167	2579	53781	174986	8132	355045
5	5244	12	96	187	2932	10172	18643
Total	9493672	35777	83409	299091	249134	21169	10182252

1988 1998 0 to 30m

Category	1988 0	1	2	3	4	5	Total
0	10113273	90	5717	6364	504	13	10125961
1	116	94	90	6	0	0	306
2	9266	122	6574	1584	22	0	17568
3	10818	29	5776	6783	105	0	23511
4	5799	5	1820	5858	861	2	14345
5	219	0	51	199	83	9	561
Total	10139491	340	20028	20794	1575	24	10182252

1988 1998 30 to 90m

Category	1988 0	1	2	3	4	5	Total
0	9991212	402	7850	18123	2647	125	10020359
1	671	785	311	19	0	0	1786
2	14936	695	11314	5450	135	0	32530
3	30388	134	10290	28833	1057	0	70702
4	22936	45	3924	21013	6584	7	54509
5	1089	2	134	529	543	69	2366
Total	10061232	2063	33823	73967	10966	201	10182252

1988 1998 90 to 150m

Category	1988 0	1	2	3	4	5	Total
0	10002759	707	4402	18812	4290	238	10031208
1	1522	1575	407	17	0	0	3521
2	7978	1028	4648	4663	123	0	18440
3	30490	148	3345	32786	1908	1	68678
4	27944	55	1476	17087	10805	16	57383
5	1602	3	85	287	865	180	3022
Total	10072295	3516	14363	73652	17991	435	10182252

1988 1998 150 to 600m

Category	1988 0	1	2	3	4	5	Total
0	9420302	2724	10217	43722	15567	1140	9493672
1	13384	18886	3408	98	1	0	35777
2	30499	8398	24823	19368	318	3	83409
3	122444	917	9484	154308	11928	10	299091
4	122252	462	3443	55411	67358	208	249134
5	11192	280	198	939	5557	3003	21169
Total	9720073	31667	51573	273846	100729	4364	10182252

Appendix C. CrossTab Results. Green is positive change, red is negative, and yellow is no change.